ANNUAL REVIEWS

Annual Review of Nuclear and Particle Science

High-Energy Multimessenger Transient Astrophysics

Kohta Murase[1,2] and Imre Bartos[3]

[1]Department of Physics, Department of Astronomy and Astrophysics, and Center for Particle and Gravitational Astrophysics, Institute for Gravitation and the Cosmos, Pennsylvania State University, University Park, Pennsylvania 16802, USA; email: murase@psu.edu

[2]Center for Gravitational Physics, Yukawa Institute for Theoretical Physics, Kyoto University, Kyoto 606-8502, Japan

[3]Department of Physics, University of Florida, Gainesville, Florida 32611, USA; email: imrebartos@ufl.edu

ANNUAL REVIEWS CONNECT

www.annualreviews.org

- Download figures
- Navigate cited references
- Keyword search
- Explore related articles
- Share via email or social media

Annu. Rev. Nucl. Part. Sci. 2019. 69:477–506

The *Annual Review of Nuclear and Particle Science* is online at nucl.annualreviews.org

https://doi.org/10.1146/annurev-nucl-101918-023510

Copyright © 2019 by Annual Reviews. All rights reserved

Keywords

neutrinos, gravitational waves, γ-rays, cosmic rays, multimessenger astrophysics

Abstract

The recent discoveries of high-energy cosmic neutrinos and gravitational waves from astrophysical objects have led to a new era of multimessenger astrophysics. In particular, electromagnetic follow-up observations triggered by these cosmic signals have proved to be highly successful and have brought about new opportunities in time-domain astronomy. We review high-energy particle production in various classes of astrophysical transient phenomena related to black holes and neutron stars, and discuss how high-energy emission can be used to reveal the underlying physics of neutrino and gravitational-wave sources.

Annu. Rev. Nucl. Part. Sci. 2019.69:477-506. Downloaded from www.annualreviews.org
Access provided by University of Florida - Smathers Lib - Gainesville on 04/01/20. For personal use only.

Contents

Annu. Rev. Nucl. Part. Sci. 2019.69:477-506. Downloaded from www.annualreviews.org
Access provided by University of Florida - Smathers Lib - Gainesville on 04/01/20. For personal use only.

1. INTRODUCTION

The new era of high-energy multimessenger astrophysics began with two recent breakthrough discoveries: (*a*) the discovery of astrophysical high-energy neutrinos by the IceCube experiment in Antarctica (1, 2) and (*b*) the direct detection of gravitational waves from the merger of two black holes by the Laser Interferometer Gravitational-Wave Observatory (LIGO) (3). These detections are also great triumphs of technological development for cosmic observations.

The feasibility of time-domain multimessenger astrophysics has been demonstrated by broadly coordinated observation campaigns in 2017 and 2018. These led to the discovery of gravitational waves from the neutron star merger event GW170817, associated with the short γ-ray burst (GRB) 170817A and the kilonova (also known as a Li–Paczynski nova or macronova) event AT 2017gfo (4, 5). The successful detection of electromagnetic counterparts at different wavelengths in follow-up observations strongly supports the concordance picture of double neutron star mergers and short GRBs, and kilonova emission is consistent with heating by the decay of heavy radioactive nuclei. Another milestone detection was that of the high-energy neutrino event IceCube-170922A, with energy of ∼0.1–1 PeV. Follow-up observations revealed its association with a flaring blazar, TXS 0506+056, and enabled the determination of its multiwavelength spectral energy distribution (SED), including the GeV–TeV γ-ray band (6). The interpretation of IceCube-170922A is still under debate, and confirmation by further observations will be important. Both of these success stories clearly demonstrate the potential of multimessenger approaches, which combine information from different types of particles and waves (photons,

neutrinos, gravitational waves, and cosmic rays) to reveal the origin of and physical processes behind high-energy astrophysical phenomena.

Neutrinos are elusive neutral fermions. In the Standard Model, there are three types of neutrinos: electron (ν_e), muon (ν_μ), and tau (ν_τ). They have tiny but finite masses, as was established by the observations of neutrino oscillation among the three generations. Aside from gravity, they interact with matter only via the weak force. Consequently, gigantic detector volumes are required to detect astrophysical neutrino signals.

In the MeV energy range, astrophysical neutrinos are produced mainly as a result of nuclear reactions, the best-known examples of which are solar and supernova neutrinos. Neutrinos from the Sun were first measured by the Homestake experiment (7), which led to the so-called solar neutrino problem—a large discrepancy between the then predicted and the measured neutrino flux from the Sun. The phenomenon of neutrino oscillation resolved this problem and confirmed the standard model of the Sun. Supernova neutrinos were discovered in the wake of a nearby supernova, SN 1987A, by multiple water Cherenkov detectors around the globe (e.g., 8).

High-energy neutrinos, with energies beyond the GeV range, are produced by relativistic protons or ions through hadronic interactions with matter or radiation. Detection of high-energy cosmic neutrinos is crucial for determining the origin of cosmic rays—which is one of the greatest mysteries in particle astrophysics. Cosmic rays are deflected by intergalactic magnetic fields, preventing us from pinpointing the location of their production site. High-energy photons can be produced by other mechanisms that do not involve cosmic-ray ions, and sufficiently high-energy γ-rays that are more likely to be hadronic are subject to electromagnetic interactions with lower-energy photons. These facts limit the use of the electromagnetic channel in probing cosmic-ray sources. High-energy neutrinos serve as a more direct probe of cosmic particle accelerators, through which we can reveal their acceleration processes even in dense environments such as supernovae.

Large-scale detectors are needed to detect high-energy cosmic neutrinos. Currently operating and near-future detectors include IceCube, a cubic-kilometer detector at the South Pole (9); KM3Net, a cubic-kilometer detector under construction in the Mediterranean (10), which is a successor of ANTARES, also in the Mediterranean (11); and the Baikal Deep Underwater Neutrino Telescope in Russia (12).

In contrast to high-energy particles, which are accelerated in energetic outflows, gravitational waves are produced by the birth and dynamics of compact objects, especially black holes and neutron stars (13–16). Detectable gravitational waves require the nonaxisymmetric acceleration of large amounts of matter, virtually ruling out any noncompact source. The strongest expected source of gravitational waves is the merger of black holes and neutron stars. To date, this is the only process from which gravitational waves have been detected (17). Such mergers can emit a few percent of the rest mass of the merging objects in the form of gravitational waves, accounting for up to a few times $M_\odot c^2$ energy for stellar-mass black holes and approximately $10^{-2}\ M_\odot c^2$ for binary neutron stars. Gravitational-wave emission is weakly anisotropic; the strongest emission along the binary's orbital axis is approximately 1.5 times higher than the emission in the average direction. Another astrophysical process with sufficient matter and acceleration for substantial gravitational-wave emission is stellar core collapse. The collapse of a massive star can cause a neutron star to be formed. Gravitational waves are expected first from the violent collapse and then from the so-called bounce of the matter after it reaches neutron star densities (18, 19). In the aftermath of the collapse, dynamical and dissipative instabilities can grow in the newly formed neutron star. In particular, if the progenitor star has high rotation, instabilities in the rapidly rotating neutron star can produce significant deviations from axisymmetry as well as numerous gravitational waves (15, 20). Depending on simulated models, gravitational waves from stellar core collapse are expected to

Annu. Rev. Nucl. Part. Sci. 2019.69:477-506. Downloaded from www.annualreviews.org
Access provided by University of Florida - Smathers Lib - Gainesville on 04/01/20. For personal use only.

be detectable for Galactic sources with advanced gravitational-wave detectors (18). However, if the rotational energy of the newly formed neutron star, or additional energy from fallback accretion, can be converted efficiently into gravitational waves, then core-collapse events could be detectable at up to tens of megaparsecs with advanced detectors (15).

The aim of this review is to summarize the current status and future prospects of multimessenger particle astrophysics, with a focus on transient sources of high-energy messengers. We begin by introducing high-energy particle production processes in Section 2. In Section 3 we present an overview of the current observational status and ongoing efforts of high-energy multimessenger transient sources. In Section 4 we discuss different transient source models and our current understanding of the underlying emission processes in these events. We present a brief outlook for the future of the field and conclude in Section 5.

2. HIGH-ENERGY RADIATION PROCESSES

2.1. Cosmic-Ray Acceleration

Nonthermal emission is ubiquitous in astrophysical processes. The fact that cosmic rays are observed in a wide energy range from MeV to ultrahigh (>EeV) energies means that charged particles can gain energy through some process.

Among various possible mechanisms, the most popular is the Fermi acceleration mechanism, originally proposed by Enrico Fermi (21). In this mechanism, charged particles gain energy stochastically via multiple interactions with scatterers. Astrophysical shocks provide a viable setup in order for this type of particle acceleration to work. Ions can be reflected by magnetic fields at the shock. While most of the particles are eventually advected to the far downstream, some of them can gain energy via scattering by electromagnetic waves in both the upstream and the downstream. In this diffusive shock acceleration mechanism (22, 23), a fraction of the energy of converging bulk flows can eventually be converted into the nonthermal energy of cosmic rays.

The diffusive shock acceleration is not the only promising mechanism, and various mechanisms such as stochastic acceleration by turbulence and magnetic reconnections have been discussed in the literature. In any case, the particles have to be confined in the system, and the fundamental necessary condition is called the Hillas condition (24),

$$\varepsilon < ZerB(v/c), \qquad 1.$$

where ε is the particle energy, Ze is the particle charge, r is the system size, B is the magnetic field strength, and v is the characteristic velocity scale (i.e., the shock velocity for the diffusive shock acceleration mechanism). For relativistic sources,

$$\varepsilon < \Gamma Zel'B', \qquad 2.$$

where l' is the comoving system size, B' is the comoving magnetic field strength, and Γ is the Lorentz factor. In reality, one has to take into account various cooling processes to evaluate the maximum energy of cosmic rays, but the details depend on the properties of the sources.

If particle acceleration occurs in relativistic outflows such as GRB jets, the Hillas condition can be rewritten as (25, 26)

$$L_B > \frac{1}{2}\Gamma^2 c\left(\frac{\varepsilon}{Ze}\right)^2 \sim 2\times 10^{46}\,\mathrm{erg\,s^{-1}}\,\Gamma^2(\varepsilon/Z\,10^{20.5}\,\mathrm{eV})^2, \qquad 3.$$

where L_B is the magnetic luminosity of the outflow. This equation implies that accelerators of ultrahigh-energy cosmic rays (UHECRs) must be powerful. The number of candidate sources is

Annu. Rev. Nucl. Part. Sci. 2019.69:477-506. Downloaded from www.annualreviews.org
Access provided by University of Florida - Smathers Lib - Gainesville on 04/01/20. For personal use only.

rather limited, and the most promising ones are extragalactic transient sources such as GRBs and flares of active galactic nuclei (AGN).

2.2. Hadronic Processes

High-energy cosmic rays interact with matter and radiation via hadronuclear and photohadronic interactions, respectively. Hadronuclear interactions are governed mainly by inelastic pp scatterings, in which neutrinos and hadronic γ-rays are produced via $p+p \to N(\pi^+,\pi^-,\pi^0)+X \to N(\nu_\mu+\bar{\nu}_\mu+\nu_e+e^+,\nu_\mu+\bar{\nu}_\mu+\bar{\nu}_e+e^-,2\gamma)+X$. Interactions above baryon resonances are dominated by multipion production, leading to the ratio $\pi^+{:}\pi^-{:}\pi^0 \approx 1{:}1{:}1$, where $\pi^\pm$ are charged pions and π^0 is a neutral pion. Although the inelastic pp cross section gradually increases with energy, using the approximate constancy with $\sigma_{pp} \sim 30$ mb and proton inelasticity with $\kappa_{pp} \sim 0.5$, the effective optical depth to pp interactions is given by

$$f_{pp}[\varepsilon_p] \approx \kappa_{pp}\sigma_{pp}ct_{\rm int}n_N, \qquad 4.$$

where $t_{\rm int}$ is the interaction time and n_N is the nucleon number density. For example, in the case of supernova shocks with size r and velocity v, cosmic rays interact with target gas while they are confined and advected to the far downstream, so one expects $t_{\rm int} \approx r/v$. In the case of engine-driven supernovae, if cosmic rays from the engine travel through the ejecta almost rectilinearly, then $t_{\rm int} \approx r/c$ is expected.

Neutrinos and hadronic γ-rays can also be coproduced via photomeson production, $p+\gamma \to N(\pi^+,\pi^-,\pi^0)+X \to N(\nu_\mu+\bar{\nu}_\mu+\nu_e+e^+,\nu_\mu+\bar{\nu}_\mu+\bar{\nu}_e+e^-,2\gamma)+X$, which is characterized by its effective optical depth, $f_{p\gamma}$. We consider a relativistic source with a target photon spectrum, $n_{\varepsilon_t'}$ (where $\varepsilon_t' \approx \varepsilon_t/\delta$ is the target photon energy in the comoving frame). If we approximate the spectrum by $\varepsilon'_t n_{\varepsilon_t'} = n_0'(\varepsilon'_t/\varepsilon'_0)^{1-\beta}$ with $\beta(>1)$ the power-law photon index and ε'_0 the reference energy, $f_{p\gamma}$ is given by (e.g., 27)

$$f_{p\gamma}[\varepsilon_p] \approx \eta_{p\gamma}[\beta]\hat{\sigma}_{p\gamma}l'n_0'(\varepsilon_p'/\tilde{\varepsilon}'_{p\gamma 0})^{\beta-1}, \qquad 5.$$

where $\eta_{p\gamma}[\beta] \approx 2/(1+\beta)$, $\hat{\sigma}_{p\gamma} \approx \kappa_{p\gamma}\sigma_\Delta(\Delta\bar{\varepsilon}_\Delta/\bar{\varepsilon}_\Delta) \sim 0.7\times10^{-28}\,{\rm cm}^2$ is the attenuation cross section $\kappa_{p\gamma} \sim 0.2, \sigma_\Delta \sim 5\times10^{-28}{\rm cm}^2, \bar{\varepsilon}_\Delta \sim 0.2$ GeV, $\bar{\varepsilon}_\Delta \sim 0.3$ GeV, $\tilde{\varepsilon}'_{p\gamma 0} = 0.5m_pc^2\bar{\varepsilon}_\Delta/\varepsilon'_0$, and l' is the comoving size. This estimate is valid when meson production is dominated by the Δ resonance and direct pion production.

In either pp or $p\gamma$ reactions, high-energy neutrinos are produced mostly as a result of pion and muon decay, and the neutrino energy fluence is written as

$$E_\nu^2\phi_\nu \approx \frac{1}{4\pi d^2}\frac{3K}{4(1+K)}f_{pp/p\gamma}\frac{\mathcal{E}_{\rm cr}}{\mathcal{R}_{\rm cr}[\varepsilon_p]}, \qquad 6.$$

where ϕ_ν is the neutrino fluence, d is the distance to the source, $\mathcal{E}_{\rm cr}$ is the energy carried by cosmic rays, and $\mathcal{R}_{\rm cr}$ is a conversion factor from the bolometric energy to the differential energy of cosmic rays. Also, K is a factor representing the ratio of charged pions to neutral pions, where $K \approx 1$ and $K \approx 2$ for $p\gamma$ and pp interactions, respectively. Realistically, pions and muons can be subject to various cooling processes, which modify the resulting neutrino spectra. Thus, more generally, theoretical predictions for neutrino and γ-ray spectra are model dependent.

The meson production processes are among the hadronic processes that involve strong interactions. In contrast, there exist purely electromagnetic processes such as the Bethe–Heitler process and proton synchrotron radiation. The γ-rays originating from electromagnetic processes are also classified as hadronic components, because cosmic-ray ions are involved.

Annu. Rev. Nucl. Part. Sci. 2019.69:477-506. Downloaded from www.annualreviews.org
Access provided by University of Florida - Smathers Lib - Gainesville on 04/01/20. For personal use only.

2.3. Leptonic Processes

γ-Rays can be produced by leptonic processes as well as hadronic ones. Charged particles that relativistically move in magnetic fields emit synchrotron emission. The characteristic synchrotron energy is

$$\varepsilon_\gamma^{\rm syn} \approx 1.5\Gamma\gamma_e'^2\hbar\frac{eB'}{m_e c} \sim 200\,{\rm eV}\,\Gamma(\gamma_e'/10^5)^2(B'/1\,{\rm G}), \quad 7.$$

where γ_e' is the Lorentz factor of relativistic electrons in the comoving frame. For example, it is widely accepted that a low-energy component of the blazar SED is interpreted as synchrotron emission (28).

High-energy electrons and photons interact via Compton scattering, $\gamma e \to \gamma e$. In the astrophysical context, γ-rays can be produced by the inverse Compton process, in which low-energy photons gain energy via upscattering by relativistic electrons. In the Thomson regime, where the photon energy in the electron rest frame is less than $m_e c^2$, we have

$$\varepsilon_\gamma^{\rm IC} \approx 2\gamma_e'^2\varepsilon_{\rm tar} \sim 20\,{\rm GeV}\,(\gamma_e'/10^5)^2(\varepsilon_{\rm tar}/1\,{\rm eV}). \quad 8.$$

where $\varepsilon_{\rm tar}$ is the energy of target photons. The Klein–Nishina effect is important at sufficiently high energies. The cross section is suppressed when the photon energy in the electron rest frame exceeds $\sim m_e c^2$. If target photons originate from synchrotron emission by primarily accelerated electrons, the process is called synchrotron self-Compton emission. If they originate elsewhere, the resulting emission is called external inverse Compton emission. In the case of blazars, the external photons can come from an accretion disk, a broad-line region, or a dust torus (28).

In the so-called leptonic scenario, observed γ-ray emission is attributed to inverse Compton radiation by primary electrons (or positrons). The electron luminosity and the magnetic field strength can be determined simultaneously through modeling of the SED.

2.4. Electromagnetic Cascades

Sufficiently high-energy γ-rays can interact with low-energy photons via the two-photon annihilation process, $\gamma\gamma \to e^+e^-$. Its optical depth is given by

$$\tau_{\gamma\gamma}[\varepsilon_\gamma] \approx \eta_{\gamma\gamma}(\beta)\sigma_{\rm T} l'(\varepsilon_t' n_{\varepsilon_t'})|_{\varepsilon_t'=m_e^2c^4/\varepsilon_\gamma'}, \quad 9.$$

where $\sigma_{\rm T} \simeq 6.65 \times 10^{-25}$ cm^2 is the Thomson cross section, ε_t' is the target photon energy in the comoving frame, and $\eta_{\gamma\gamma}(\beta) \simeq 7/[6\beta^{5/3}(1+\beta)]$ for $1 < \beta < 7$ (29), which is of the order of 0.1. There is a correspondence between $p\gamma$ and $\gamma\gamma$ optical depths. The typical γ-ray energy is given by $\varepsilon_\gamma \approx \Gamma^2 m_e^2 c^4 \varepsilon_t^{-1}$, and we have (e.g., 27)

$$\tau_{\gamma\gamma}[\varepsilon_\gamma^c] \approx \frac{\eta_{\gamma\gamma}\sigma_{\gamma\gamma}}{\eta_{p\gamma}\hat{\sigma}_{p\gamma}} f_{p\gamma}[\varepsilon_p] \sim 10\left(\frac{f_{p\gamma}[\varepsilon_p]}{0.01}\right), \quad 10.$$

where ε_γ^c is the γ-ray energy corresponding to the resonance proton energy satisfying $\varepsilon_\gamma^c \approx 2m_e^2c^2\varepsilon_p/(m_p\bar{\varepsilon}_\Delta) \sim {\rm GeV}(\varepsilon_\nu/25\,{\rm TeV})$. The above equation implies that efficient emitters of 10–100 TeV neutrinos are predicted to be "dark" as the sources of GeV–TeV γ-rays (27). Conversely, GeV–TeV bright γ-ray sources may not be ideal as the sources of neutrinos at 10–100 TeV energies.

If the intrasource $\gamma\gamma$ optical depth is larger than unity, high-energy γ-rays are attenuated inside the source. However, energy conservation implies that high-energy pairs produced via $\gamma\gamma \to e^+e^-$

Annu. Rev. Nucl. Part. Sci. 2019.69:477-506. Downloaded from www.annualreviews.org
Access provided by University of Florida - Smathers Lib - Gainesville on 04/01/20. For personal use only.

keep generating lower-energy photons via synchrotron and inverse Compton processes, known as an electromagnetic cascade. The cascade can be induced by either primary ions or primary electrons, and it is important for powerful accelerators such as GRBs and blazars. Although the details of an emergent spectrum depend on source parameters, a broad SED is formed as a generic trend, and the minimal proton-induced cascade fluence satisfies

$$\int^{\varepsilon_\gamma^{\rm S-cut}} {\rm d}\varepsilon_\gamma \, (\varepsilon_\gamma \phi_\gamma^{\rm S-cas}) \approx \int_{0.5\varepsilon_\gamma^{\rm S-cut}} {\rm d}\varepsilon_\nu \left(\frac{4+K}{3K} \varepsilon_\nu \phi_\nu \right), \qquad 11.$$

where $\varepsilon_\gamma^{\rm S-cut}$ is the energy at which the $\gamma\gamma$ optical depth is unity and $\phi_\gamma^{\rm S-cas}$ is the fluence of γ-rays cascaded inside the source. More generally, there are additional contributions to cascade emission from the Bethe–Heitler and proton synchrotron processes. Efficient cascades are unavoidable in photon-rich sources, for which X-ray and γ-ray observations are critical to examine bright neutrino sources. The relevance of intrasource cascades has been demonstrated in the modeling of TXS 0506+056 (30–34).

γ-Rays capable of leaving the sources interact with cosmic radiation fields, including the cosmic microwave background and extragalactic background light. Except for ultrahigh energies, intergalactic cascades are governed by the two-photon annihilation and inverse Compton scattering processes (35). Note that if the target photon field is thermal, the intrasource $\gamma\gamma$ optical depth decreases at high energies, allowing only high-energy γ-rays to escape from the sources (27, 36).

The spectrum of intergalactic electromagnetic cascades is nearly universal and is expressed as (35, 37)

$$\varepsilon_\gamma^2 \phi_\gamma^{\rm IG-cas} \propto \begin{cases} \varepsilon_\gamma^{1/2} & (\varepsilon_\gamma \le \varepsilon_\gamma^{\rm br}), \\ \varepsilon_\gamma^{2-\beta} & (\varepsilon_\gamma^{\rm br} < \varepsilon_\gamma < \varepsilon_\gamma^{\rm IG-cut}), \end{cases} \qquad 12.$$

where $\varepsilon_\gamma^{\rm IG-cut}$ is the cutoff energy due to the extragalactic background light, $\phi_\gamma^{\rm IG-cas}$ is the fluence of γ-rays cascaded in intergalactic space, $\varepsilon_\gamma^{\rm br} \approx 2(\varepsilon_\gamma^{\rm IG-cut}/m_e c^2)^2 \varepsilon_{\rm CMB}$, $\varepsilon_{\rm CMB}$ is the typical energy of the cosmic microwave background photons, and $\beta \sim 2$ is the index that depends on details of cascades. For a TeV γ-ray source located at a redshift of $z \sim 1$, the cutoff due to the extragalactic background light typically lies in the 0.1 TeV range, leading to a prediction of a flat energy spectrum down to ~30 MeV in the observer frame (37).

The multimessenger connection among the diffuse cosmic particle (neutrinos, γ-rays, and cosmic rays) fluxes is crucial in order to reveal the origin of high-energy cosmic neutrinos. If IceCube neutrinos originate from inelastic pp collisions and the sources are optically thin to $\gamma\gamma \to e^+e^-$ up to TeV energies (which are valid for star-forming galaxies and galaxy clusters), then the fact that the isotropic γ-ray background flux, measured by *Fermi*-LAT (38), is comparable to the diffuse neutrino flux leads to the conclusion that the intrinsic spectral index at the sources has to be $s < 2.1$–2.2 (39).

3. MULTIMESSENGER OBSERVATIONAL STATUS

3.1. High-Energy Neutrino Observations and Electromagnetic Counterpart Searches

The detection of high-energy cosmic neutrinos with PeV energies was first reported at the Neutrino 2012 conference in Kyoto, Japan (1). The two events were found in the search for extremely high-energy neutrinos. The follow-up analysis of high-energy starting events led to 4σ evidence of high-energy cosmic neutrinos (2), and accumulated data have established their

Annu. Rev. Nucl. Part. Sci. 2019.69:477-506. Downloaded from www.annualreviews.org
Access provided by University of Florida - Smathers Lib - Gainesville on 04/01/20. For personal use only.

existence (40). Individual sources have not been definitively identified, so the IceCube flux can be regarded as the diffuse neutrino flux (or intensity). The measured diffuse neutrino flux is $E_\nu^2 \Phi_\nu \sim 3 \times 10^{-8}\,\mathrm{GeV\,cm^{-2}\,s^{-1}\,sr^{-1}}$ for all three flavors. These neutrinos consist of contributions from all sources that exist along the line of sight from the Earth, which is often called the astrophysical neutrino background. North-sky searches for track events induced by muon neutrinos suggest a similar energy flux with a hard spectrum of $\Phi_\nu \propto E_\nu^{-2.1}$ (41). In contrast, analyses of medium-energy starting events and shower events, which are sensitive to neutrinos below 100 TeV, indicated a steeper spectrum of $\Phi_\nu \propto E_\nu^{-2.5}$ (40, 42). The different spectral indices might indicate the existence of distinct components, and a large diffuse neutrino flux of $E_\nu^2 \Phi_\nu \sim 10^{-7}\,\mathrm{GeV\,cm^{-2}\,s^{-1}\,sr^{-1}}$ suggests a population of hidden neutrino sources arising from the tension with the isotropic γ-ray background flux (27).

The nondetection of point sources or high-energy multiplet sources (from which more than one neutrino originate from a given position in the sky) implies that the source population responsible for the bulk of IceCube neutrinos is unlikely to be a rare class of astrophysical sources. Rather, abundant sources such as starburst galaxies, galaxy clusters/groups, and radio-quiet AGN are favored. Next-generation detectors such as IceCube-Gen2 will be essential in order to identify the main origin of IceCube neutrinos (43).

In contrast, transient sources will be detectable with the current IceCube if a bright burst or flare occurs. Time and space coincidence will also allow us to significantly reduce atmospheric backgrounds. This advantage has been exploited for stacking searches for neutrino emission from GRBs. The nondetection of coincident events between neutrinos and GRBs has led to important constraints on cosmic-ray acceleration in GRBs (44, 45). Stacking searches for neutrino–supernova associations have also been performed (46, 47). Multiplet searches are also powerful for the transient neutrino sources (48, 49).

Neutrino-triggered follow-up observations provide an alternative way to identify the sources of high-energy neutrinos (50, 51). The real-time alert system in IceCube was developed for this purpose. To detect subthreshold multimessenger signals, the Astrophysical Multimessenger Network Observatory has attempted to combine multimessenger information in real time (52). The feasibility of such a neutrino-triggered follow-up approach was best demonstrated by the observations of TXS 0506+056 that coincided with IceCube-170922A (6), as presented in **Figure 1**. Within the error circle of this high-energy neutrino event, several blazar candidates were identified by the Kanata Telescope, and one of them turned out to be a *Fermi*-LAT blazar in the high state. Several X-ray sources were identified through follow-up observations by *Swift*, and also NuSTAR observed TXS 0506+056. This source was also observed by the MAGIC γ-ray telescope. The significance of the association with the γ-ray flare was $\sim 3\sigma$, which is insufficient to claim a discovery. Interestingly, however, archival analyses of past track data for TXS 0506-056 revealed a neutrino flare in 2014–2015 (53). Although associated γ-ray flares were not found for this past neutrino flare event, the $\sim 4\sigma$ significance presented intriguing evidence that this blazar is a potential neutrino source.

3.2. Gravitational-Wave Observations and Electromagnetic Counterpart Searches

Gravitational-wave searches have been used to initiate and to follow up electromagnetic observations since the era of first-generation gravitational-wave detectors began more than a decade ago (54–59). With the limited sensitivity of the initial gravitational-wave detectors, which were able to detect binary neutron star mergers out to approximately 20 Mpc, common detection was possible, but not probable. Nevertheless, gravitational-wave searches triggered by electromagnetic

Annu. Rev. Nucl. Part. Sci. 2019.69:477-506. Downloaded from www.annualreviews.org
Access provided by University of Florida - Smathers Lib - Gainesville on 04/01/20. For personal use only.

Annu. Rev. Nucl. Part. Sci. 2019.69:477-506. Downloaded from www.annualreviews.org
Access provided by University of Florida - Smathers Lib - Gainesville on 04/01/20. For personal use only.

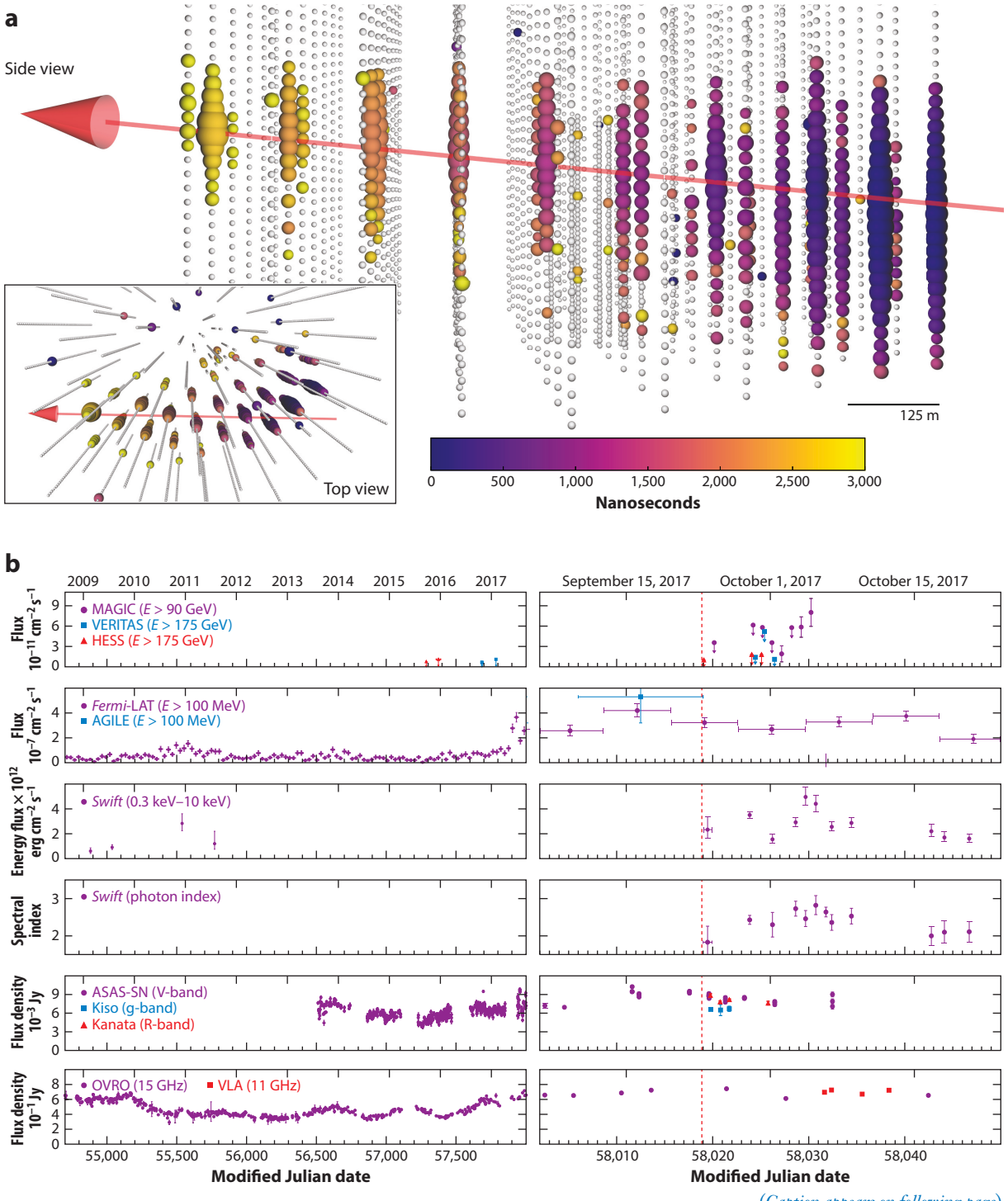

(Caption appears on following page)

Figure 1 (*Figure appears on preceding page*)

Multimessenger observations of TXS 0506+056 associated with the high-energy neutrino event IceCube-170922A. (*a*) Image of the neutrino-induced track event. (*b*) Multiwavelength light curves. The vertical dashed line indicates the timing of the detection of IceCube-170922A. Figure adapted with permission from Reference 6.

Annu. Rev. Nucl. Part. Sci. 2019.69:477-506. Downloaded from www.annualreviews.org
Access provided by University of Florida - Smathers Lib - Gainesville on 04/01/20. For personal use only.

observations resulted in a few astrophysically meaningful constraints, for example, by indicating that a short GRB, GRB 070201, that was directionally coincident with M31 could not have been produced by a compact binary merger (57).

Gravitational-wave observations with advanced detectors brought about a wide-scale, broadband electromagnetic follow-up effort. The first gravitational-wave discovery of a binary black hole merger, GW150914, on September 14, 2015, was followed up by more than 60 observing facilities covering radio, optical, near-IR, X-ray, and γ-ray wavelengths (60).

One of these facilities, the Gamma-ray Burst Monitor on the *Fermi* satellite (*Fermi*-GBM), reported the detection of a spatially and temporally coincident, albeit marginal, short GRB 0.4 s after the binary merger (61, 62), although the significance of this detection is debated (63). A marginal short GRB counterpart was also detected later for another binary black hole merger discovered through gravitational waves, GW170104, in this case by the *AGILE* satellite (64). However, this GRB was not observed by other detectors (65), and an unrelated, directionally overlapping long GRB complicated matters (66).

The electromagnetic follow-up campaign to identify gravitational waves finally triumphed with the observation of the binary neutron star merger GW170817 (4, 5, 67). This merger was discovered simultaneously by LIGO/Virgo and by *Fermi*-GBM, the former through gravitational waves within minutes and the latter through its short GRB counterpart within seconds after the event (67, 68). The spatial and temporal overlap between these two detections was rapidly recognized and initiated a broadband, multimessenger search for emission from the source.

Figure 2 presents a visual summary of the follow-up effort to detect GW170817/GRB 170817A. Less than 11 h after the merger, its optical kilonova emission was found, first by the Swope Telescope (69). X-ray and radio emission from the GRB afterglow were detected only with a large delay 9 and 16 days after the merger, respectively, by the *Chandra X-ray Observatory* and by the Jansky Very Large Array (70, 71).

GW170817/GRB 170817A provided a wealth of unique information on high-energy emission from binary neutron star mergers that changed our GRB paradigm, which would not have been possible without the observation of both gravitational waves and electromagnetic emission. First, the binary merger occurred at a large inclination angle of 15°–40° (72). Prior to this discovery, GRB observations had been anticipated only for smaller angles. Second, detailed afterglow observations revealed that the outflow is structured with a narrow energetic component along the orbital axis and weaker emission at greater inclinations (73–79). Such a structured emission had not been incorporated into GRB population studies prior to GW170817. This could mean either that GRB 170817A is a rare event type (80) or that a population of nearby GRBs observed at high inclination angles and without reconstructed distances may exist (81–83). It would also mean that a nonnegligible fraction of future gravitational-wave observations of binary neutron star mergers will be accompanied by detectable GRBs, promising frequent high-energy multimessenger discoveries.

3.3. Coincidence Searches for Gravitational Waves and Neutrinos

The search for common sources of gravitational waves and neutrinos has a long history, going back to the first extrasolar neutrino source, SN 1987A (8, 84). In the era of interferometric gravitational-wave observatories, joint searches have been investigated in detail, starting around

Annu. Rev. Nucl. Part. Sci. 2019.69:477-506. Downloaded from www.annualreviews.org
Access provided by University of Florida - Smathers Lib - Gainesville on 04/01/20. For personal use only.

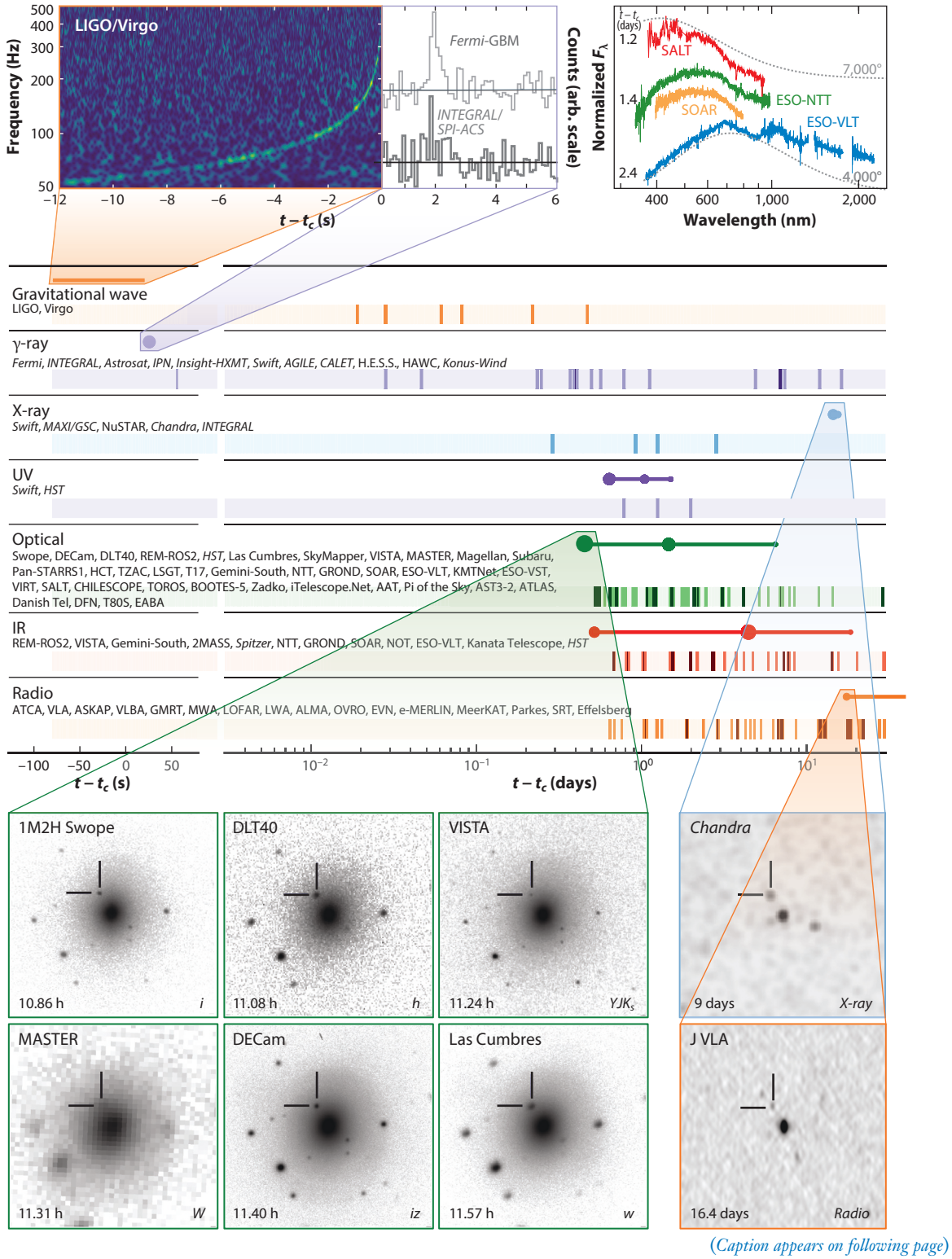

(Caption appears on following page)

Figure 2 (*Figure appears on preceding page*)

Multimessenger observations of GW170817. Figure adapted from Reference 5/CC BY 3.0.

Annu. Rev. Nucl. Part. Sci. 2019.69:477-506. Downloaded from www.annualreviews.org
Access provided by University of Florida - Smathers Lib - Gainesville on 04/01/20. For personal use only.

2006 (85–91). No such joint detection has been made so far, making this the next frontier of the multimessenger puzzle.

This type of search consists of two distinct categories, based on the type of neutrino signal. The first category consists of sources producing nonthermal, high-energy neutrinos with GeV energies and beyond, and the second category consists of thermal, MeV neutrinos. In this review, we restrict our discussion to the first category, which is closely connected to high-energy emission.

The first searches for common sources of gravitational waves and high-energy neutrinos were performed with the initial LIGO and Virgo detectors, as well as with the partially completed IceCube and ANTARES detectors (92–94). These analyses targeted event candidates for which neither the gravitational-wave nor the neutrino data were sufficiently significant to confidently indicate an astrophysical signal.

Advanced LIGO's first observing run, from September 2015 until January 2016, brought about the first detections of gravitational waves (95) and with them the first targeted searches for high-energy neutrinos from established gravitational-wave sources via the IceCube, ANTARES, and Pierre Auger observatories (96–98). All three binary black hole mergers from this period, discovered via gravitational waves, were followed up by neutrino searches. Neutrino emission from these events was constrained to isotropic-equivalent energies lower than $\sim 10^{51}$–10^{54} erg, assuming a neutrino spectrum $\mathrm{d}N/\mathrm{d}E \propto E^{-2}$. The spread in this emission constraint is due to the large localization uncertainty of gravitational waves, as the sensitivity of neutrino detectors can significantly change over the source directions allowed by gravitational waves.

Gravitational-wave and high-energy neutrino data obtained during Advanced LIGO's first observing run were also analyzed in searches of events that remained below the detection threshold in individual data channels (99). While no joint event was discovered, these searches represented a sensitivity improvement of more than two orders of magnitude over similar searches carried out with earlier-generation detectors. **Figure 3** shows the observational constraints derived from these analyses. For realistic source rates of $<10^5$ Gpc^{-3} year^{-1}, these constraints limit the source population in the strong emission regime of gravitational-wave energy $\mathcal{E}_{\rm GW} \gtrsim 10^{-2}\ M_\odot c^2$ and isotropic-equivalent neutrino energy $\mathcal{E}_\nu \gtrsim 10^{51}$ erg.

During Advanced LIGO/Virgo's second observing run, from November 2016 to August 2017, searches for coincident neutrinos were performed in near real time with IceCube and ANTARES, and over a period of approximately a day with Pierre Auger, following every gravitational-wave detection (100, 101). This rapid analysis was motivated by the fact that a coincident neutrino would significantly aid electromagnetic observations. While gravitational-wave localizations are typically limited to hundreds of square degrees (102), high-energy neutrinos can be reconstructed to subdegree precision, substantially reducing the number of electromagnetic foreground transients and the sky area that observatories need to survey in order to identify electromagnetic emission from the source. Since both gravitational waves and neutrinos are expected to be emitted by the main sources of interest within minutes (89), multimessenger identification on a similar timescale can aid in the search for electromagnetic emission such as a GRB afterglow or kilonova, which can be observable over a longer period.

Advanced LIGO/Virgo's second observing run was crowned by the multimessenger discovery of the binary neutron star merger GW170817, a few days before the end of the run. This detection also represented a unique opportunity for high-energy neutrino searches. While no coincident neutrino was detected, the joint analysis of the participating observatories, ANTARES, IceCube, and Pierre Auger, was used to compute a joint constraint on neutrino emission from

Annu. Rev. Nucl. Part. Sci. 2019.69:477-506. Downloaded from www.annualreviews.org
Access provided by University of Florida - Smathers Lib - Gainesville on 04/01/20. For personal use only.

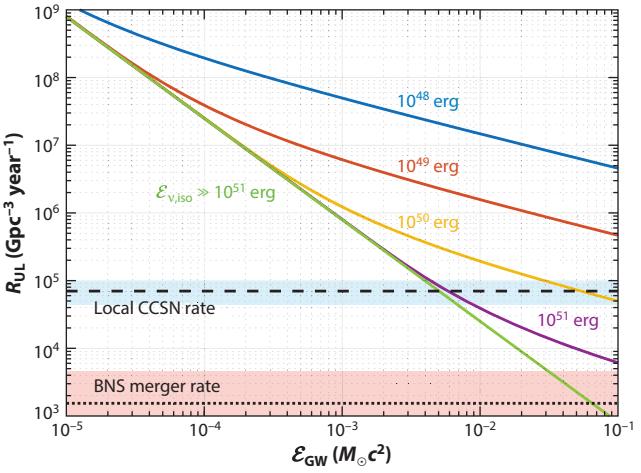

Figure 3

Constraints on rate density of high-energy neutrino transients as a function of energy released as gravitational waves. Here $\mathcal{E}_{\nu,\mathrm{iso}}$ is the released energy of neutrinos, and $\mathcal{E}_{\mathrm{GW}}$ is the released energy of gravitational waves. Abbreviations: BNS, binary neutron star; CCSN, core-collapse supernova. Adapted from Reference 99/CC BY 3.0.

the merger over nine orders of magnitude of energy, from 100 GeV to 100 EeV. **Figure 4** compares these observational constraints with selected emission scenarios. These results show that, assuming some of the optimistic emission models from short GRBs (103), we can rule out on-axis emission of optimistic scenarios related to extended emission, which is consistent with the large viewing angle inferred both from the gravitational-wave data and from afterglow observations (72, 79). Although the current afterglow observations are not enough to determine the entire jet structure (104), the detection of GW170817 also indicated that high-energy emission may be

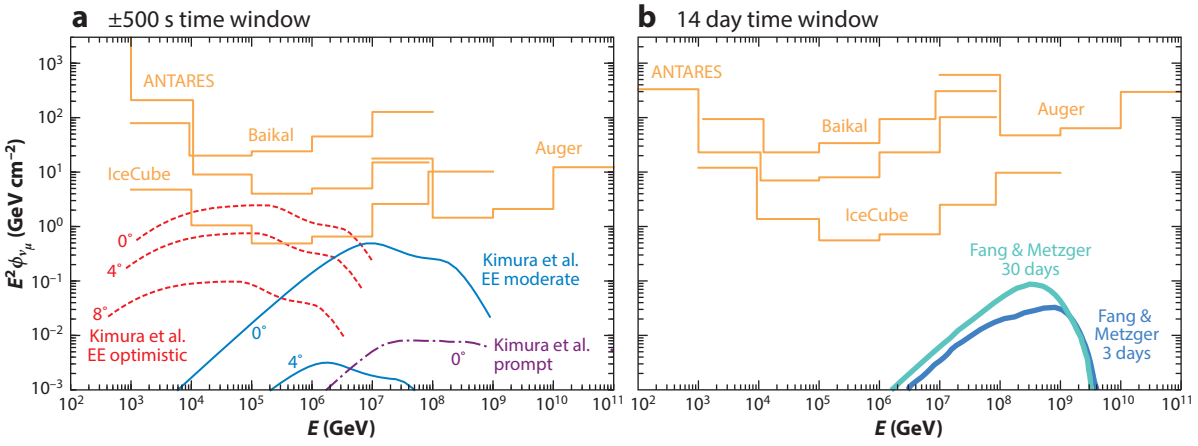

Figure 4

High-energy neutrino fluence upper limits as a function of neutrino energy for the binary neutron star merger GW170817, based on data from ANTARES, IceCube, and the Pierre Auger Observatory. (*a*) Limits for a ±500 s time window around the merger. (*b*) Limits over a 2-week period. Several model predictions are shown for comparison (103, 107). Abbreviation: EE, extended emission. Figure adapted from Reference 100/CC BY 3.0 and Reference 108.

Annu. Rev. Nucl. Part. Sci. 2019.69:477-506. Downloaded from www.annualreviews.org
Access provided by University of Florida - Smathers Lib - Gainesville on 04/01/20. For personal use only.

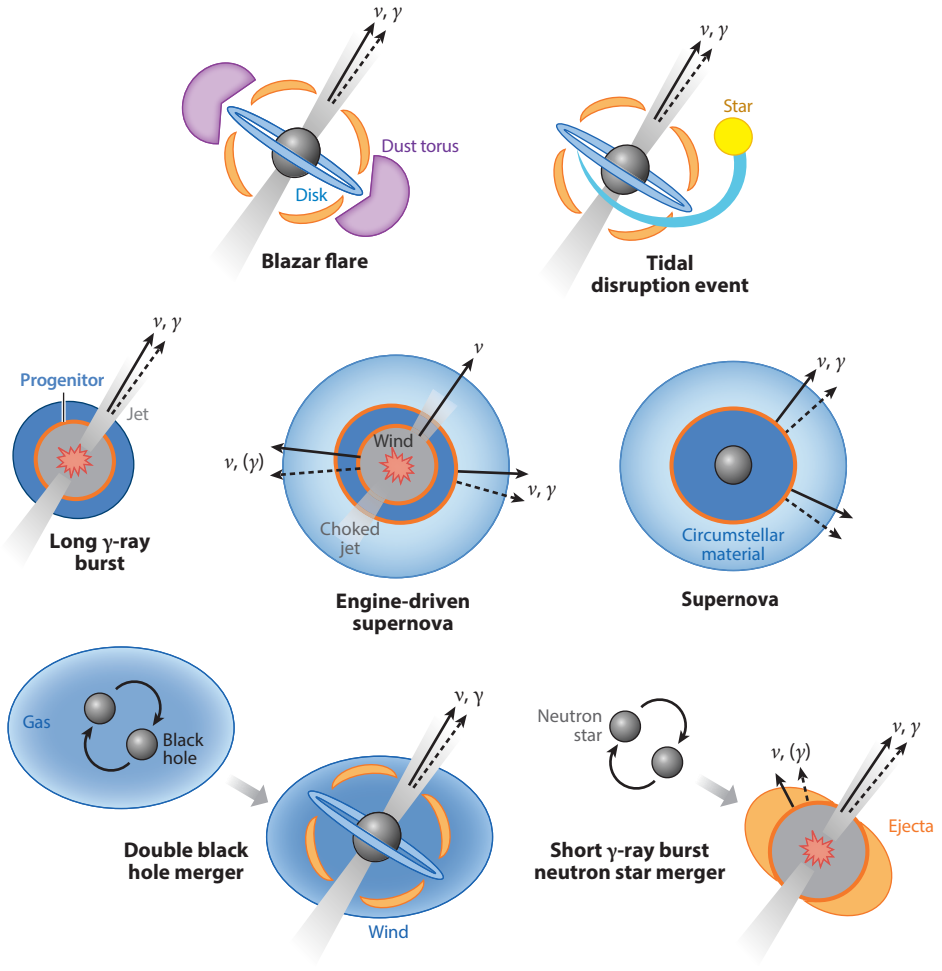

Figure 5

Schematic picture of various high-energy multimessenger transients.

observable at greater viewing angles than previously anticipated (82, 105, 106), making nearby binary mergers an interesting target for upcoming joint observing periods.

4. SOURCE MODELS

In this section, we discuss several possible sources of neutrinos and gravitational waves, which can be accompanied by high-energy emission. **Figure 5** depicts the high-energy emission mechanisms, and **Table 1** lists these sources along with some characteristic numbers.

4.1. Blazar Flares

In general, blazars are highly variable objects that show broadband spectra from the radio, optical, X-ray, and γ-ray bands. In the standard leptonic scenario for SEDs, the low-energy and high-energy humps are explained by synchrotron emission and inverse Compton radiation from

Table 1 List of multimessenger transients that can be promising emitters of high-energy neutrinos and/or gravitational waves

Source	Rate density (Gpc^{-3} $year^{-1}$)	EM luminosity ($erg\,s^{-1}$)	Duration (s)	Typical counterpart
Blazar flare[a]	10–100	10^{46}–10^{48}	10^{6}–10^{7}	Broadband
Tidal disruption event	0.01–0.1	10^{47}–10^{48}	10^{6}–10^{7}	Jetted (X)
	100–1,000	$10^{43.5}$–$10^{44.5}$	$>10^{6}$–10^{7}	Tidal disruption event (optical, UV)
Long GRB	0.1–1	10^{51}–10^{52}	10–100	Prompt (X, γ)
Short GRB	10–100	10^{51}–10^{52}	0.1–1	Prompt (X, γ)
Low-luminosity GRB	100–1,000	10^{46}–10^{47}	1,000–10,000	Prompt (X, γ)
GRB afterglow		$<10^{46}$–10^{51}	>1–10,000	Afterglow (broadband)
Supernova (II)	10^{5}	10^{41}–10^{42}	$>10^{5}$	Supernova (optical)
Supernova (Ibc)	3×10^{4}	10^{41}–10^{42}	$>10^{5}$	Supernova (optical)
Hypernova	3,000	10^{42}–10^{43}	$>10^{6}$	Supernova (optical)
NS merger	300–3,000	10^{41}–10^{42}	$>10^{5}$	Kilonova (optical/IR)
		10^{43}	$>10^{7}$–10^{8}	Radio flare (broadband)
BH merger	10–100	?	?	?
WD merger	10^{4}–10^{5}	10^{41}–10^{42}	$>10^{5}$	Merger nova (optical)

[a]Blazar flares such as the 2017 flare of TXS 0506+056 are assumed for the demonstration.
Abbreviations: BH, black hole; EM, electromagnetic; GRB, γ-ray burst; NS, neutron star; WD, white dwarf.

nonthermal electrons, respectively. For BL Lacertae (BL Lac) objects that typically belong to a low-luminous class of blazars, seed photons for inverse Compton scattering are supplied mainly by the electron synchrotron process. In contrast, flat-spectrum radio quasars (FSRQs) tend to be more luminous; it is believed that the external inverse Compton process is important for FSRQs. The origin of external target photon fields is under debate; it may be an accretion disk, broad-line regions, a surrounding dusty torus, or the sheath region of a structured jet.

The high-energy hump could be dominated by a hadronic component, which is the so-called lepto-hadronic scenario. The γ-rays could be attributed to either cosmic-ray-induced electromagnetic cascade emission or ion synchrotron radiation (28). In the former case, the lepto-hadronic scenario predicts that the γ-ray flux is comparable to the neutrino flux. The latter case usually requires strong magnetic fields and does not necessarily accompany efficient neutrino production.

In either explanation of high-energy γ-rays, it is reasonable to consider a hybrid picture in which both cosmic-ray ions and electrons are coaccelerated in the source. Target photons are not only synchrotron photons from primary leptons but also external radiation fields (109, 110). For example, let us consider a scattered accretion disk field. The effective optical depth to $p\gamma$ interactions is given by

$$f_{p\gamma} \approx \hat{n}_{\rm ext}\hat{\sigma}_{p\gamma}r_{\rm ext} \sim 0.01\left(\frac{\tau_{\rm sc}}{0.1}\right)\left(\frac{r_{\rm sc}}{10^{18}\,{\rm cm}}\right)^{-1}\left(\frac{L_{\rm AD}}{10^{46.5}\,{\rm erg\,s^{-1}}}\right)\left(\frac{\varepsilon_{\rm AD}}{10\,{\rm eV}}\right)^{-1}, \qquad 13.$$

where $\hat{n}_{\rm ext}$ is the external radiation density in the black hole rest frame, $\tau_{\rm sc}$ is the optical depth to Thomson scattering for disk photons, $r_{\rm sc}$ is the size of the scattering region, $L_{\rm AD}$ is the radiation luminosity of the accretion disk, and $\varepsilon_{\rm AD}$ is the typical energy of the disk photons.

The detection of IceCube-170922A, associated with TXS 0506+056, provided new insights into the origin of γ-rays. In this case, electromagnetic cascades inside the source play a crucial role in extracting implications for the source physics (30–34). High-energy neutrinos provide a smoking gun of cosmic-ray acceleration, so one would naïvely expect that neutrino detection would

Annu. Rev. Nucl. Part. Sci. 2019.69:477-506. Downloaded from www.annualreviews.org
Access provided by University of Florida - Smathers Lib - Gainesville on 04/01/20. For personal use only.

Annu. Rev. Nucl. Part. Sci. 2019.69:477-506. Downloaded from www.annualreviews.org
Access provided by University of Florida - Smathers Lib - Gainesville on 04/01/20. For personal use only.

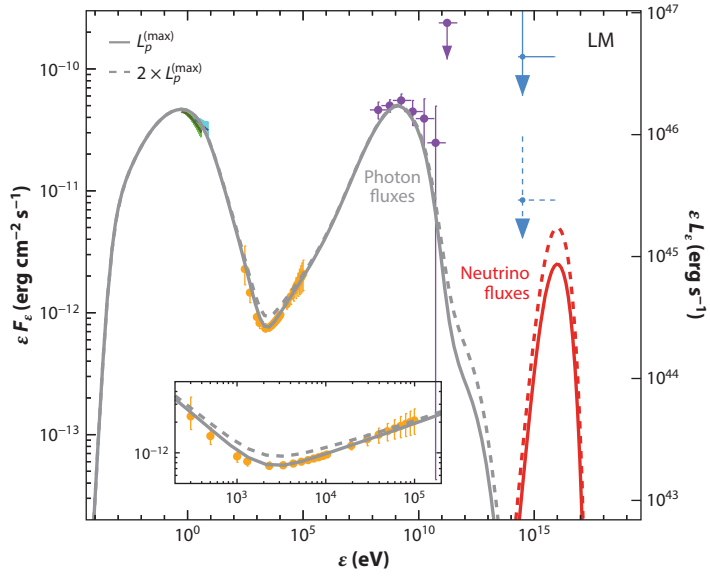

Figure 6

Spectral energy distribution of TXS 0506+056 during the flare (31). The neutrino flux estimated by real-time alerts is from Reference 6. Abbreviation: LM, leptonic model. Figure adapted with permission from References 6 and 31.

support the lepto-hadronic scenario. However, this is not the case. The SED of this blazar clearly shows the peak below 3×10^{14} Hz and the dip in the X-ray range (31), strongly constraining the hadronic components. The neutrino flux is basically limited by the X-ray flux (**Figure 6**). Thus, proton-induced cascades cannot provide a viable explanation for the γ-rays. Proton synchrotron emission can account for the γ-ray component, but the neutrino flux in the range of 0.1–1 PeV is predicted to be too low to explain the best-fit flux level of the IceCube data. Thus, ironically, the leptonic scenario is supported if IceCube-170922A originates from the flare of this blazar.

In addition, the fact that γ-rays were detected by MAGIC implies that the effective optical depth to $p\gamma$ interactions has to be very small; that is, the required cosmic-ray power is too large. The cascade problem is even more serious for the neutrino flare event that occurred in 2014–2015 (32, 111, 112). These challenges may indicate that multizone models are necessary (32).

4.2. Tidal Disruption Events

A star can be swallowed by a supermassive black hole located in the center of a galaxy. While the star is approaching the black hole, it can be tidally disrupted by the gravitational force, which occurs at the tidal disruption radius. Approximately half of the mass is ejected, whereas the other half forms an accretion disk and eventually falls back into the black hole. It is believed that the accretion initially proceeds as a super-Eddington mode and then becomes sub-Eddington. Resulting transients are observed as tidal disruption events (TDEs).

Some TDEs possess relativistic jets that can be launched from the black hole–accretion disk system. *Swift* J1644+57 is thought to be such a jetted TDE. Strong nonthermal X-rays were observed, with a typical duration of $t_{\rm dur} \sim 10^6$ s. The bolometric radiation energy is $\mathcal{E}_\gamma \sim 10^{54}$ erg, implying that the beam-corrected energy is $\mathcal{E}_j \sim 10^{51}$–$10^{52}$ erg. Theoretically, it is widely discussed that the jets are powered by the Blandford–Znajek mechanism (113).

Cosmic-ray acceleration in TDEs was proposed as a "giant flare" scenario (114), and the associated neutrino emission has also been calculated (115–119). The discovery of *Swift* J1644+57 revealed that jetted TDEs are strong X-ray sources (120). High-energy protons efficiently interact with these X-rays. Equation 5 implies that the effective $p\gamma$ optical depth is

$$f_{p\gamma}[\varepsilon_p] \sim 1 \frac{(L_\gamma^b/10^{47.5}\,\mathrm{erg\,s^{-1}})}{(r/10^{14.5}\,\mathrm{cm})(\Gamma/10)^2(\varepsilon_\gamma^b/1\,\mathrm{keV})}\left(\frac{\varepsilon_p}{\varepsilon_p^b}\right)^{\beta-1}, \qquad 14.$$

where L_γ^b is the luminosity at the peak energy ε_γ^b, and β is the photon index. Equation 14 implies that jetted TDEs can be efficient neutrino emitters given that cosmic rays are accelerated in the jet.

The nondetection of high-energy neutrinos from *Swift* J1644+57 implies that the energy carried by the cosmic rays is less than $\sim 30\mathcal{E}_\gamma$. Their contribution to the diffuse neutrino flux is expected to be $\lesssim$10% (117, 118), which is consistent with the limit from the absence of high-energy neutrino multiplets (118). If the disrupted star is a white dwarf, then TDEs are expected to be promising gravitational-wave sources (121, 122).

4.3. Supernovae

A massive star with a stellar mass of $\gtrsim 8M_\odot$ leads to a supernova explosion. During the gravitational collapse of a progenitor core, the central temperature increases, and most of the gravitational binding energy, which is estimated as $\mathcal{E}_\mathrm{G} \approx \left(GM_\mathrm{ns}^2/R_\mathrm{ns}\right) \sim 3 \times 10^{53}\,\mathrm{erg}\,(M_\mathrm{ns}/1M_\odot)^2\left(R_\mathrm{ns}/10^6\,\mathrm{cm}\right)^{-1}$ (where M_ns is the remnant mass and R_ns is the radius), is extracted by thermal neutrinos. Supernovae are known to be MeV neutrino emitters, as was established by the detection of SN 1987A (8, 84).

High-energy neutrinos with energies beyond the GeV or TeV range can be produced in two ways. First, cosmic rays are accelerated by a supernova shock, and the neutrinos are produced through interaction with the ambient material. This situation is analogous to that of supernova remnants. Second, cosmic rays are supplied by outflows from the engine, as discussed further in Sections 4.4 and 4.5 with a focus on GRBs and engine-driven supernovae.

In the early stages of supernova remnants, most of the energy is in kinetic form, and the energy fraction carried by cosmic rays is expected to be negligibly small. However, recent observations of extragalactic supernovae have shown that significant mass losses always occur before the explosion (123). The most spectacular examples are Type IIn supernovae, which show clear indications of interactions with the circumstellar material (CSM). Some of them, which are usually classified as Type IIn supernovae, indicate that the CSM mass reaches $M_\mathrm{cs} \sim 1$–$10\,M_\odot$, given that the CSM is spherical. Even Type II-P supernovae, which are most common among core-collapse supernovae, may have a significant CSM mass of $M_\mathrm{cs} \sim 10^{-3}$–$10^{-1}\,M_\odot$.

As the shock propagates, photons eventually break out, and the shock becomes collisionless and is not mediated by radiation. One may then expect the diffusive shock acceleration mechanism to operate as in supernoval remnants. The accelerated protons should interact with gas via pp interactions, and the effective optical depth for inelastic pp interactions is estimated to be

$$f_{pp} \approx \kappa_{pp}\sigma_{pp}(\varrho_\mathrm{cs}/m_H)r_s(c/v_\mathrm{s}) \sim 1\,(M_\mathrm{cs}/10^{-2}\,M_\odot)(r_\mathrm{s}/10^{14}\,\mathrm{cm})^{-2}(v_\mathrm{s}/3{,}000\,\mathrm{km\,s^{-1}})^{-1}, \qquad 15.$$

where r_s is the shock radius, v_s is the shock velocity, and ϱ_cs is the CSM density. Equation 15 implies that high-energy neutrino and γ-ray production occurs efficiently at early times. **Figure 7** depicts neutrino light curves for various types of supernovae. IceCube can detect ~100–1,000 high-energy

Annu. Rev. Nucl. Part. Sci. 2019.69:477-506. Downloaded from www.annualreviews.org
Access provided by University of Florida - Smathers Lib - Gainesville on 04/01/20. For personal use only.

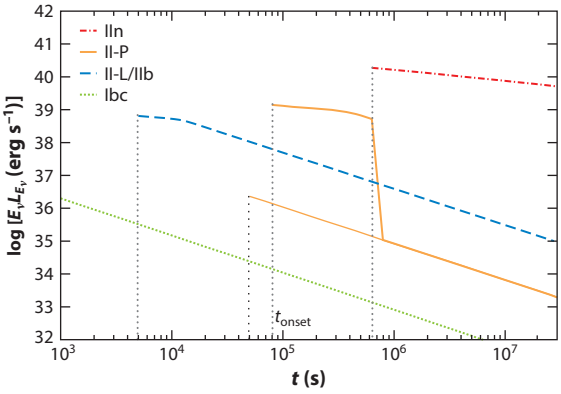

Figure 7

High-energy neutrino light curves expected for various types of core-collapse supernovae. The neutrino light curve was depicted at $E_\nu = 1$ TeV. Figure adapted with permission from Reference 124.

neutrinos from a Type II-P supernova (124), if the next Galactic supernova occurs at $d \sim 10$ kpc. Detection of high-energy emission from extragalactic supernovae requires stronger CSM interactions, which can be expected for Type IIn supernovae (125, 126). Searches for GeV–TeV γ-ray emission have also been performed, but the constraints are still consistent with theoretical predictions (127–129).

Some Type Ibc supernovae with a relativistic velocity component—transrelativistic supernovae that are often associated with low-luminosity GRBs—can also be neutrino and γ-ray emitters owing to interactions with the CSM (see References 130 and 131 for more details).

Core-collapse supernovae represent one of the promising directions of gravitational-wave studies (132–135). Because core-collapse events are hidden from electromagnetic observations by the stellar material, only gravitational waves and thermal MeV neutrinos are able to carry information directly from the collapse to the observer. Nevertheless, most emission models and numerical simulations predict gravitational-wave emission that is detectable by Advanced LIGO/Virgo for core-collapse supernovae within the Milky Way (18, 19). Without a rapidly rotating core, the gravitational-wave frequency will be characteristic of the newly formed proto–neutron star's oscillation frequencies, while the gravitational-wave amplitude may be characteristic of the accretion rate (135). Much stronger gravitational-wave emission can be produced by rapidly rotating cores, in which dynamical and dissipative instabilities can result in a rotating nonaxisymmetric structure that can radiate away some of the proto–neutron star's angular momentum in gravitational waves (18). The amount of angular momentum available for gravitational-wave radiation can be further increased by fallback accretion (136). If the conversion of angular momentum is efficient, gravitational waves from core-collapse supernovae with rapidly rotating cores can be detected out to tens of megaparsecs (137–139).

4.4. Long γ-Ray Bursts

Long GRBs are among the brightest explosive astrophysical phenomena in the Universe. Their isotropic-equivalent luminosities in γ-rays reach $L_{\rm iso} \sim 10^{51}$–10^{52} erg s^{-1} with a duration of $t_{\rm dur} \sim$ 10–100 s. These observations imply that the isotropic-equivalent γ-ray energy is $\mathcal{E}_{\rm iso} \sim 10^{53}$ erg. This value is comparable to the isotropic-equivalent kinetic energy of GRB jets, which is inferred from multiwavelength observations of the GRB afterglow emission. The outflows are thought to

Annu. Rev. Nucl. Part. Sci. 2019.69:477-506. Downloaded from www.annualreviews.org
Access provided by University of Florida - Smathers Lib - Gainesville on 04/01/20. For personal use only.

be collimated, and the true energy of the jet is $\mathcal{E}_j \sim 10^{51}$ erg if the jet opening angle is $\theta_j \sim 0.1$. The central engine of the GRB jets and the properties of the jet are unknown. It is believed that the jet is powered by a black hole with an accretion disk or a strongly magnetized neutron star (a so-called magnetar). In the former case, the energy budget is limited by the rotation energy of a spinning black hole, $\mathcal{E}_{\rm BH-rot} = \left[1 - \sqrt{\frac{1+\sqrt{1-a_*^2}}{2}}\right] M_{\rm BH} c^2 \sim 4 \times 10^{53}\,{\rm erg}\,(\frac{M_{\rm BH}}{3\,M_\odot})$, where $a_* = a/M_{\rm BH}$ and $a_* \sim 0.7$ is assumed in the last estimate. In the latter case, the energy source is the rotation energy of the remnant star, which is given by $\mathcal{E}_{\rm NS-rot} = \frac{1}{2} I \left(\frac{2\pi}{P_i}\right)^2 \sim 2 \times 10^{52}\,{\rm erg}\,(\frac{M_*}{1.4\,M_\odot})\,(\frac{R_*}{10\,{\rm km}})^2\,(\frac{P_i}{1\,{\rm ms}})^{-2}$, where $I \approx 0.35 M_* R_*^2$ is the inertia of momentum, M_* is the stellar mass, and R_* is the stellar radius. Neutrino and gravitational-wave signals can provide us with valuable information about the central engine and jet composition.

Prompt γ-ray emission originates from internal dissipation in a relativistic jet with a bulk Lorentz factor of $\Gamma \sim 100$–$1{,}000$, and the γ-ray energy spectrum has a peak around $\varepsilon_\gamma^b \sim 1$ MeV. The emission mechanism has been under debate for many years. In the classical picture (140, 141), the observed γ-rays are attributed to synchrotron radiation from nonthermal electrons that are accelerated inside a jet. Particles may be accelerated by internal shocks, which are thought to be mildly relativistic. However, efficient shock acceleration does not occur if the shock is relativistic and strongly magnetized, and magnetic reconnections are also considered to be a promising mechanism. In either case, not only electrons but also ions will be accelerated in the jet, and high-energy neutrinos can be produced via $p\gamma$ interactions. Through the use of Equation 5, we estimate the effective optical depth to $p\gamma$ interactions to be

$$f_{p\gamma}[\varepsilon_p] \sim 0.01 \frac{(L_\gamma^b/10^{51.5}\,{\rm erg\,s^{-1}})}{(r/10^{14.5}\,{\rm cm})(\Gamma/10^{2.5})^2(\varepsilon_\gamma^b/1\,{\rm MeV})} \left(\frac{\varepsilon_p}{\varepsilon_p^b}\right)^{\beta-1}. \quad 16.$$

For GRBs, $\beta \sim 1$ and $\beta \sim 2$–3 for the low- and high-energy spectral portions, respectively. The typical energy of neutrinos is predicted to be 0.1–1 PeV (142), which is the ideal energy range for IceCube. The importance of multipion production and other, higher resonances has been investigated (143, 144). **Figure 8** shows an example of the latest theoretical calculations (145). For GRB-like transients, stacking analyses are powerful, and the contribution to the diffuse neutrino flux is constrained to be less than ~1% (45, 146). However, the possibility that GRBs are responsible for the observed UHECR flux has not yet been excluded, and further observations are necessary (147–149). Also, dimmer populations of bursts, such as low-luminosity GRBs, are missing in the GRB samples used in the stacking analyses, so they could still make a significant contribution to the diffuse neutrino flux (50, 150–152), as well as to the UHECR flux (153–156).

Alternatively, the observed prompt γ-rays could be attributed to quasi-thermal, photospheric radiation. Various photospheric models have been described in the literature (140, 141). Proposed subphotospheric dissipation mechanisms include internal shocks, magnetic reconnections, and collisions with neutron-loaded outflows. Whereas high-energy neutrino production around the photosphere is possible (158–160), efficient acceleration of cosmic rays at shocks deep inside the photosphere is unlikely when the hydrodynamical shock is collisional or mediated by radiation (161). (A strong subshock is, in principle, possible if the shock is magnetized, but cosmic-ray ion acceleration is inefficient for strongly magnetized, perpendicular shocks.) In contrast, even if cosmic-ray acceleration does not occur, neutrinos can naturally be produced by neutrons. Naturally, neutrons are entrained into the jet. The neutrons are initially coupled with protons, but the decoupled neutron flow is eventually caught by a faster flow, causing inelastic np collisions (162, 163). Alternatively, internal shocks between compound flows are accompanied by dissipation via inelastic collisions. In either case, quasi-thermal neutrinos are expected, and the typical energy of

Annu. Rev. Nucl. Part. Sci. 2019.69:477-506. Downloaded from www.annualreviews.org
Access provided by University of Florida - Smathers Lib - Gainesville on 04/01/20. For personal use only.

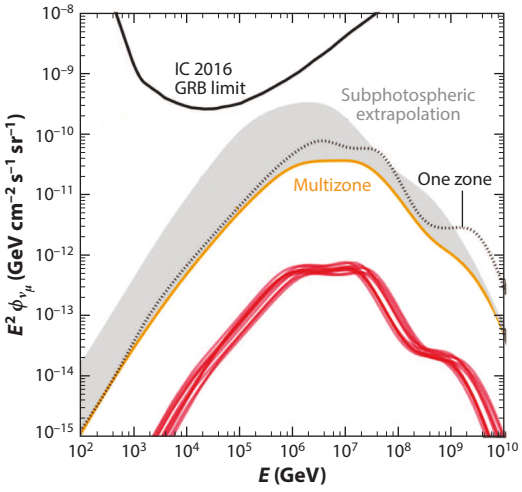

Figure 8

Aggregated neutrino fluxes from γ-ray burst (GRB) prompt emission. The figure shows the differential limit from IceCube as well as a possible contribution from subphotospheric neutrino emission. IC 2016 refers to the IceCube 2016 upper limit, which was calculated using their latest reported detector effective area and exposure in a stacked GRB search using tracks coming from the Northern Hemisphere (157). Adapted from Reference 145.

neutrinos is $\varepsilon_\nu \sim 10$–100 GeV. Such neutrinos could be detected in more detailed analyses using the DeepCore data (164, 165).

Despite their typically large distance from the Earth, the progenitors of some long GRBs may produce detectable gravitational waves, which requires that the collapsing stellar core that will produce the GRB first form a rapidly rotating proto–neutron star. Some of the proto–neutron stars formed in stellar core collapse may survive sufficiently long to develop dynamical or even dissipative instabilities, which deform the proto–neutron stars and result in the emission of gravitational waves. If a significant fraction of the proto–neutron stars' rotational energy can be converted into gravitational waves, this emission could be detectable by Advanced LIGO/Virgo out to tens of megaparsecs (15). Very massive stars, however, can collapse without a supernova explosion (the so-called collapsar scenario), leaving virtually no time for a proto–neutron star to form and emit gravitational waves. Possible gravitational-wave emission in this scenario may come from fragmentation of the accretion disk (166–168), the collapsing star (169, 170), anisotropic neutrino emission (171), or GRB jets (172), although these emission processes are currently uncertain. Alternatively, some long GRBs may be produced directly by rapidly rotating proto–neutron stars with strong magnetic fields instead of a black hole–accretion disk system. In this scenario, the proto–neutron star survives for a longer time, is fast-rotating, and is accreting additional matter, all of which favors gravitational-wave emission (173).

4.5. Engine-Driven Supernovae

GRBs are caused by a relativistic jet that successfully breaks out from the progenitor star. However, the jet will not necessarily penetrate. A sufficiently low-power jet may naturally become "choked" inside a progenitor or dense CSM (174–177). Such failed GRBs may be observed as so-called engine-powered supernovae. Some of them are thought to become low-luminosity GRBs, whose properties are intermediate between those of supernovae and GRBs. Indeed, there have been

Annu. Rev. Nucl. Part. Sci. 2019.69:477-506. Downloaded from www.annualreviews.org
Access provided by University of Florida - Smathers Lib - Gainesville on 04/01/20. For personal use only.

observations of such objects in which the jet marginally fails or succeeds and a transrelativistic component is seen in the ejecta velocity distribution. They are likely to be more common than canonical high-luminosity GRBs. The γ-ray emission mechanism is under debate; the most popular scenario is that it originates from shock breakout of the relativistic ejecta in a dense CSM (178). As discussed above, high-energy neutrino and γ-ray emission may occur around the shock breakout.

Choked jets embedded in the stellar material or CSM are promising sources of high-energy neutrinos, given that cosmic rays are accelerated by the jets. Importantly, the system is calorimetric in the sense that sufficiently high-energy cosmic rays are fully depleted for neutrino and γ-ray production; that is, $\min[1, f_{p\gamma}] \approx 1$. The emitted neutrinos are called orphan neutrinos (if the jet is deeply choked and little γ-ray emission is produced) or precursor neutrinos (if accompanied by delayed γ-ray emission). However, cosmic-ray acceleration is suppressed when the shock is radiation mediated. Radiation largely smears the upstream structure, leading to a much weaker subshock, and the energy carried by low-energy cosmic rays becomes small. This so-called radiation constraint suggests that canonical high-luminosity GRBs are unlikely to be emitters of high-energy neutrinos (161). Low-power GRBs, which can be produced if the jet is intrinsically weak and/or if the stellar material is extended, allow cosmic-ray acceleration and associated neutrino production. They have also been suggested to be the main sources of high-energy neutrinos in the 10–100 TeV range (151, 161, 179). As noted above, these medium-energy neutrinos imply the existence of hidden neutrino sources.

Energy injection from the central engine does not have to be caused by relativistic jets that are collimated outflows. Winds from a pulsar or accretion disk around a black hole can also power the ejecta and the resulting observed emissions. In particular, a fast-rotating pulsar or magnetar has been actively discussed as the central engine for various types of supernovae as well as GRBs (e.g., 180–182). Long-lived pulsars or magnetars are also intriguing sources of gravitational waves, and high-energy counterpart searches have attracted much interest.

Pulsar winds are expected to be Poynting dominated and can form a pair of forward and reverse shocks via interaction with the supernova ejecta. Pulsar wind nebulae such as the Crab Nebula have broadband, nonthermal spectra from the radio, optical, X-ray, and γ-ray wavelengths. Detailed modeling of the nonthermal nebular emissions indicates that the plasma is carried by electron–positron pairs, and a significant fraction of these pairs are accelerated around the termination shock.

It is natural to expect that embryonic pulsar wind nebulae are also efficient accelerators of electrons and positrons. In this case, bright X-ray counterparts can be expected as month-to-year transients (183). In particular, hard X-rays serve as powerful probes of pulsar-driven supernovae (181, 184), but there has been no indication of candidate supernovae, including superluminous ones (185). γ-Rays have greater penetration power, and strong γ-ray emission in the GeV–TeV range is produced by upscattering of supernova photons. GeV γ-rays are detectable up to nearby supernovae within 100 Mpc; these are potential targets for *Fermi*-LAT (184), and searches have been performed (186). Their TeV γ-ray counterparts are interesting targets for imaging atmospheric Cherenkov telescopes such as MAGIC, VERITAS (Very Energetic Radiation Imaging Telescope Array System), H.E.S.S. (High Energy Stereoscopic System), and CTA (Cherenkov Telescope Array), but they are subject to intrasource attenuation by supernova photons.

Some ions can potentially be accelerated in the wind or around the termination shock. Even acceleration to ultrahigh energies has been suggested (187, 188). Although the details of ion acceleration by embryonic pulsar wind nebulae are unknown, possible mechanisms include surfing or wake-field acceleration. Ultrahigh-energy ions escaping from the nebula are damped in the ejecta and radiation field, and high-energy neutrinos are produced via both pp and $p\gamma$ interactions

Annu. Rev. Nucl. Part. Sci. 2019.69:477-506. Downloaded from www.annualreviews.org
Access provided by University of Florida - Smathers Lib - Gainesville on 04/01/20. For personal use only.

(189, 190). For example, the effective optical depth to pp interactions is estimated to be

$$f_{pp} \approx \kappa_{pp}\sigma_{pp}(\varrho_{\rm ej}/m_H)r_{\rm ej} \simeq 4\,(M_{\rm ej}/M_\odot)(r_{\rm ej}/10^{15}\ {\rm cm})^{-2}, \qquad 17.$$

where $r_{\rm ej}$ is the shock radius, $v_{\rm ej}$ is the shock velocity, and $\varrho_{\rm ej}$ is the ejecta density. The system is calorimetric at early times. However, because of the high density of the ejecta, pions and muons are cooled before they decay, so the neutrino flux can initially be suppressed at the highest energies. At late times, although the suppression is negligible, the neutrino flux declines following the spin-down power. Recently, this model has been applied to the fast blue optical transient AT2018cow (191).

4.6. Short γ-Ray Bursts and Neutron Star Mergers

A connection between short GRBs and neutron star mergers has been anticipated for decades (140, 192–194) and was strongly supported by the multimessenger discovery of the neutron star merger GW170817 and its GRB counterpart GRB 170817A, although the origin of the prompt γ-rays is still under debate (67). As the two neutron stars approach each other during the merger, some of their mass becomes tidally disrupted, forming a disk around the newly formed, central compact object. The central object eventually collapses into a black hole. Accretion onto the black hole from the surrounding disk then drives a relativistic outflow.

The merger of a neutron star and a black hole can also produce similar relativistic outflows to those of neutron star mergers, but only if the black hole's mass is sufficiently small ($\lesssim$10 $M_\odot$) to tidally disrupt the neutron star before merging (15, 195–202). To date, no neutron star–black hole merger has been detected with gravitational waves, constraining their rate to $\lesssim$600 Gpc^{-3} year^{-1} (17). The properties of relativistic outflows from neutron star–black hole mergers may differ from those of binary neutron star mergers due to the different black hole and ejecta masses of the two event types. In addition, a supramassive neutron star that forms in neutron star mergers can alter the outflow if it survives longer than a few milliseconds.

Neutron star mergers are among the most promising sources of gravitational waves for Earth-based interferometers such as LIGO and Virgo. At Advanced LIGO/Virgo's design sensitivity, neutron star mergers will be detectable out to approximately 200 Mpc on average (102), corresponding to a detection rate of 3–100 per year (17). Gravitational waves will confirm which nearby high-energy events resulted from neutron star mergers. In addition, Advanced LIGO/Virgo will provide the masses of the merging black holes, which in turn can be used to determine how much neutron star matter became tidally disrupted and how long the newly formed supramassive neutron star is expected to live before collapsing into a black hole. Even more could be learned by use of information from both gravitational waves and the detected electromagnetic/neutrino emission (203–205). Gravitational waves will also help constrain the equation of state of supranuclear matter (206). Finally, gravitational waves carry information about the luminosity distance of neutron star mergers, which, together with the redshift of the merger's host galaxy, provides an alternative distance ladder to constrain Hubble's constant (207).

Short GRBs produced by neutron star mergers can be distinguished from long GRBs produced by stellar core collapse by their duration, which is typically less than 2 s, and by their spectral hardness compared with that of the softer long GRBs. While the two types of GRBs have comparable peak luminosities, due to their durations short GRBs emit much less overall isotropic-equivalent energy in γ-rays, mostly within 10^{49}–10^{52} erg (194).

The discovery of the binary neutron star merger GW170817 and its GRB counterpart GRB 170817A strongly supported the existing short GRB paradigm, while also providing interesting new questions related to our understanding of the short GRB engine. In particular, the

Annu. Rev. Nucl. Part. Sci. 2019.69:477-506. Downloaded from www.annualreviews.org
Access provided by University of Florida - Smathers Lib - Gainesville on 04/01/20. For personal use only.

inclination of the orbiting binary was 15°–40° off the direction of Earth (72). The observation of γ-rays at such a high inclination angle demonstrates that the relativistic outflow is structured, with a stronger, highly beamed component along the inclination axis and a weaker emission that extends to higher angles (74, 76, 79, 208). The origin of this observed structure is not yet clear. One possibility is the interaction of the relativistic outflow with the lower-velocity, quasi-isotropic dynamical and wind ejecta (73, 75).

Short GRBs may be important sources of high-energy neutrinos, with neutrino fluxes possibly comparable to the flux of γ-rays, reaching up to $\sim 10^{51}$ erg of isotropic-equivalent energy (103, 209). Neutrino emission can be even higher if γ-rays are partially attenuated, for instance, by the dynamical ejecta surrounding the merger, which the relativistic outflow must burrow through (106). As the beamed outflow from neutron star mergers is expected to be neutron rich, the collision of relativistic protons with slower neutrons also represents an alternative mechanism to convert the outflow's kinetic energy to γ-rays and GeV neutrinos (164, 165).

Searches for GeV–TeV γ-ray emission from GRB 170817A have been conducted, but no positive signal has been found (210, 211). Some short GRBs are accompanied by extended and plateau emissions. These photons can be upscattered by relativistic electrons accelerated at the jet, and the resulting GeV–TeV γ-rays could be detected by γ-ray telescopes (105). In particular, CTA is expected to be powerful for long-lasting γ-ray counterpart searches.

4.7. Black Hole Mergers

Stellar-mass binary black hole mergers represent the primary source of gravitational waves, with detection rates that could reach one per day within the next few years (17, 102). Binary black holes may originate either from binary stellar systems that both undergo stellar collapse (212) or from dynamical encounters in galactic nuclei or globular clusters (213–217). These different formation channels result in different binary properties, such as mass, mass ratio, and spin.

Binary black hole mergers are generally not expected to result in emission other than gravitational waves. However, some of the binaries may merge in dense environments in which sufficient gas is available for accretion to produce detectable electromagnetic or neutrino emission. The observation of a possible short GRB by *Fermi*-GBM in coincidence with the binary black hole merger GW150914 could be a first hint of such an event (61; but see Reference 63). Scenarios that can cause electromagnetic and neutrino emission include mergers in the accretion disks of AGN (218–221), gas or debris remaining around the black holes from their prior evolution (222–225; but see Reference 226), and binary black hole formation inside a collapsing star (227; but see Reference 228). The electromagnetic and neutrino brightness of binary black hole mergers within these scenarios are currently not well constrained.

4.8. White Dwarf Mergers

Double white dwarf mergers are thought to be among the progenitors of Type Ia supernovae. However, the details of such violent merger processes are still under debate, and they may be observed as weaker optical transients (229). Numerical simulations suggest that white dwarf mergers can result in the ejection of material with a mass of $\sim 10^{-3}$–$10^{-2}\, M_\odot$ (230).

The magnetic luminosity of the outflows is $L_B \sim 10^{44}$–10^{46} erg s^{-1}, which can be accompanied by magnetic reconnections and particle acceleration. Following this scenario, one could expect high-energy neutrino emission from white dwarf mergers (231). Turbulence and efficient particle acceleration are expected beyond the photon diffusion radius. Given the dissipation of magnetic energy via reconnections, TeV–PeV neutrinos could be expected after the photons break out, and

Annu. Rev. Nucl. Part. Sci. 2019.69:477-506. Downloaded from www.annualreviews.org
Access provided by University of Florida - Smathers Lib - Gainesville on 04/01/20. For personal use only.

the signals may coincide with thermal emission in the optical band. These high-energy neutrinos could be used as probes of the outflow dynamics, magnetic energy dissipation, and cosmic-ray acceleration at subphotospheres. Note that the accompanying high-energy γ-rays are absorbed because of the large $\gamma\gamma$ optical depth, so these sources are among the hidden neutrino sources.

Double white dwarf mergers are important targets for low-frequency gravitational-wave observations with, for instance, LISA (232–234). Multimessenger detections will enable us to probe the merger rate, binary formation, and evolution mechanisms as well as links to explosion mechanisms such as Type Ia supernovae.

5. OUTLOOK

We have presented a review of high-energy emission processes in cosmic transients in the context of multimessenger observations. The era of these observations has just begun, and we anticipate many more discoveries in the near future. This means that the field is set to develop and change in the near future; however, we believe that this review can help guide the reader through well-established processes and show where interesting open questions currently lie. We summarize some of the main open questions below.

The physical association between neutrinos and blazar flares is currently tentative and should be confirmed by more discoveries with multimessenger observations in the near future. Observational constraints from other blazars suggest that X-ray data are critical for the SED modeling and observational monitoring of blazar flares at multiple wavelengths, especially in the X-ray band. Stacking searches with IceCube data, based on additional blazar flare samples, will provide a complementary test. Theoretical predictions indicate that FSRQs are stronger emitters of high-energy neutrinos than are BL Lac objects. The high-energy hump of the brightest FSRQs is expected to lie in the MeV range, and they are more common at higher redshifts. Thus, MeV observations with more sensitive telescopes such as AMEGO (All-sky Medium Energy Gamma-ray Observatory; see Reference 235) will be important, and the possibility that such blazars significantly contribute to the IceCube neutrino flux can be tested in the future. Searches for ultrahigh-energy neutrinos in the EeV range will also be important to determine whether or not blazars are accelerators of UHECRs.

Long GRBs and jetted TDEs are among the brightest X-ray and γ-ray transients in the Universe. Even though they are not dominant in the diffuse neutrino sky, they are still viable as the main sources of UHECRs. Thus, further dedicated searches for neutrinos from GRBs and TDEs are necessary. Long GRBs are potential sources of gravitational waves, and TDEs are also expected to be intriguing gravitational wave emitters for the disruption of a white dwarf by an intermediate black hole. Coincidence searches with gravitational waves with next-generation gravitational-wave detectors such as the Einstein Telescope and Cosmic Explorer (236, 237) will be crucial. We also note that relativistic jets of GRBs and TDEs propagate in the interstellar material and that UHECR acceleration may occur in the afterglow phase. For such neutrino afterglows, the typical energy of neutrinos is expected to be in the EeV range, and observations with next-generation neutrino detectors, such as ARA (Askaryan Radio Array), ARIANNA [Antarctic Ross Ice-Shelf Antenna Neutrino Array, which may merge into the RNO (Radio Neutrino Observatory)], GRAND (Giant Radio Array for Neutrino Detection), Trinity, and POEMMA (Probe Of Extreme Multi-Messenger Astrophysics), will be important (238).

Recent surveys in the optical and IR bands have revealed the diversity of supernovae, and some of these classes, such as superluminous supernovae and hypernovae, may share a similar type of central engine with GRBs and even fast radio bursts. Understanding the connections among these cosmic explosions will be important to reveal the mechanisms of jets and outflows, as well as the

Annu. Rev. Nucl. Part. Sci. 2019.69:477-506. Downloaded from www.annualreviews.org
Access provided by University of Florida - Smathers Lib - Gainesville on 04/01/20. For personal use only.

roles of black holes and neutron stars. They are promising sources of gravitational waves, and high-energy neutrinos and γ-rays will provide information about dense environments that cannot be probed by visible light. These types of explosions might significantly contribute to the diffuse neutrino flux, especially in the 10–100 TeV range. Not only stacking analyses but also neutrino-triggered follow-up observations will be useful to test the models. Neutrino observations with a sufficiently good angular resolution of $\sim$0.1–0.2° will be necessary (43) and could be achieved by KM3Net (10) and IceCube-Gen2 (239). Nearby supernovae, including the next Galactic supernova, will also be interesting targets as multimessenger sources. They are undoubtedly promising sources of MeV neutrinos and gravitational waves. In addition, high-energy neutrinos from Type II supernovae are detectable, and more than 100 events may be detected for the next Galactic event (124). In this sense, supernovae can be not only multimessenger but also multienergy sources, and cosmic-ray ion acceleration may be observed in real time by neutrino and γ-ray observations. Hyper-Kamiokande could observe not only MeV neutrinos but also GeV neutrinos (240).

In the next decade, there will be many events of gravitational-wave signals from black hole and/or neutron star mergers. Some short GRBs have extended and plateau emissions, so X-ray observations will be important to understand the activities of the central engine. Regarding TeV γ-ray searches, γ-ray monitors such as HAWC (High-Altitude Water Cherenkov Observatory) and SGSO (Southern Gamma-Ray Survey Observatory) (241) will enable the observation of bright γ-ray emissions during the prompt and early afterglow phases, whereas CTA (Cherenkov Telescope Array) (242) will play a role in deeper follow-up observations of gravitational-wave transients. Coincident detection of high-energy neutrinos and gravitational waves from neutron star mergers may be challenging for the current IceCube but could be achieved with next-generation neutrino detectors such as IceCube-Gen2.

DISCLOSURE STATEMENT

The authors are not aware of any affiliations, memberships, funding, or financial holdings that might be perceived as affecting the objectivity of this review.

ACKNOWLEDGMENTS

The authors thank Markus Ahlers, Christopher Berry, Kunihito Ioka, Szabolcs Marka, Peter Mészáros, Christian Spiering, and the IceCube Collaboration. The article has been approved for publication by the LIGO Scientific Collaboration under document number LIGOP1900117. The authors thank Pennsylvania State University and the University of Florida for their generous support. The work of K.M. is supported by Pennsylvania State University, the Alfred P. Sloan Foundation, and grant PHY-1620777 from the National Science Foundation. I.B. is grateful for the generous support of the University of Florida and the National Science Foundation under grant PHY-1911796.

LITERATURE CITED

1. Aartsen MG, et al. *Phys. Rev. Lett.* 111:021103 (2013)
2. Aartsen MG, et al. *Science* 342:1242856 (2013)
3. Abbott BP, et al. *Phys. Rev. Lett.* 116:061102 (2016)
4. Abbott BP, et al. *Phys. Rev. Lett.* 119:161101 (2017)
5. Abbott BP, et al. *Astrophys. J.* 848:L12 (2017)

Annu. Rev. Nucl. Part. Sci. 2019.69:477-506. Downloaded from www.annualreviews.org
Access provided by University of Florida - Smathers Lib - Gainesville on 04/01/20. For personal use only.

6. Aartsen MG, et al. *Science* 361:eaat1378 (2018)
7. Davis R. *Prog. Part. Nucl. Phys.* 32:13 (1994)
8. Koshiba M. *Phys. Rep.* 220:229 (1992)
9. Halzen F. *Nat. Phys.* 13:232 (2016)
10. Adrián-Martínez S, et al. *J. Phys. G* 43:084001 (2016)
11. Ageron M, et al. *Nucl. Instrum. Methods A* 656:11 (2011)
12. Belolaptikov IA, et al. *Astropart. Phys.* 7:263 (1997)
13. Shibata M, Taniguchi K. *Living Rev. Relativ.* 14:6 (2011)
14. Faber JA, Rasio FA. *Living Rev. Relativ.* 15:8 (2012)
15. Bartos I, Brady P, Márka S. *Class. Quantum Gravity* 30:123001 (2013)
16. Baiotti L, Rezzolla L. *Rep. Prog. Phys.* 80:096901 (2017)
17. Abbott BP, et al. arXiv:1811.12907 [astro-ph] (2018)
18. Ott CD. *Class. Quantum Gravity* 26:063001 (2009)
19. Kotake K, Sato K, Takahashi K. *Rep. Prog. Phys.* 69:971 (2006)
20. Andersson N, et al. *Gen. Relativ. Gravit.* 43:409 (2011)
21. Fermi E. *Phys. Rev.* 75:1169 (1949)
22. Drury LO. *Rep. Prog. Phys.* 46:973 (1983)
23. Blandford R, Eichler D. *Phys. Rep.* 154:1 (1987)
24. Hillas AM. *Annu. Rev. Astron. Astrophys.* 22:425 (1984)
25. Blandford RD. *Phys. Scr. T* 85:191 (2000)
26. Waxman E, Loeb A. *J. Cosmol. Astropart. Phys.* 0908:026 (2009)
27. Murase K, Guetta D, Ahlers M. *Phys. Rev. Lett.* 116:071101 (2016)
28. Böttcher M. *Galaxies* 7:20 (2019)
29. Baring MG. *Astrophys. J.* 650:1004 (2006)
30. Ansoldi S, et al. *Astrophys. J. Lett.* 863:L10 (2018)
31. Keivani A, et al. *Astrophys. J.* 864:84 (2018)
32. Murase K, Oikonomou F, Petropoulou M. *Astrophys. J.* 865:124 (2018)
33. Cerruti M, et al. *Mon. Not. R. Astron. Soc.* 483:L12 (2019)
34. Gao S, Fedynitch A, Winter W, Pohl M. *Nat. Astron.* 3:88 (2019)
35. Berezinsky VS, Smirnov AY. *Astrophys. Space Sci.* 32:461 (1975)
36. Murase K. *Phys. Rev. Lett.* 103:081102 (2009)
37. Murase K, Beacom JF, Takami H. *J. Cosmol. Astropart. Phys.* 1208:030 (2012)
38. Ackermann M, et al. *Astrophys. J.* 799:86 (2015)
39. Murase K, Ahlers M, Lacki BC. *Phys. Rev. D* 88:121301 (2013)
40. Aartsen MG, et al. arXiv:1710.01191 [hep-ph] (2017)
41. Aartsen MG, et al. *Astrophys. J.* 833:3 (2016)
42. Aartsen MG, et al. *Phys. Rev. D* 91:022001 (2015)
43. Murase K, Waxman E. *Phys. Rev. D* 94:103006 (2016)
44. Abbasi R, et al. *Nature* 484:351 (2012)
45. Aartsen MG, et al. *Astrophys. J. Lett.* 805:L5 (2015)
46. Senno N, Murase K, Mészáros P. *J. Cosmol. Astropart. Phys.* 1801:025 (2018)
47. Esmaili A, Murase K. *J. Cosmol. Astropart. Phys.* 1812:008 (2018)
48. Aartsen MG, et al. *Astron. Astrophys.* 607:A115 (2017)
49. Aartsen MG, et al. *Phys. Rev. Lett.* 122:051102 (2019)
50. Murase K, Ioka K, Nagataki S, Nakamura T. *Astrophys. J.* 651:L5 (2006)
51. Kowalski M, Mohr A. *Astropart. Phys.* 27:533 (2007)
52. Smith MWE, et al. *Astropart. Phys.* 45:56 (2013)
53. Aartsen MG, et al. *Science* 361:147 (2018)
54. Mohanty SD, et al. *Class. Quantum Gravity* 21:S765 (2004)
55. Márka S, Mohanty SD. *Nucl. Phys. B Proc. Suppl.* 138:446 (2005)
56. Piscionere J, et al. *Bull. Am. Astron. Soc.* 39:910 (2007)
57. Abbott BP, et al. *Astrophys. J.* 681:1419 (2008)

Annu. Rev. Nucl. Part. Sci. 2019.69:477-506. Downloaded from www.annualreviews.org
Access provided by University of Florida - Smathers Lib - Gainesville on 04/01/20. For personal use only.

58. Abadie J, et al. *Astron. Astrophys.* 541:A155 (2012)
59. Abadie J, et al. *Astrophys. J.* 755:2 (2012)
60. Abbott BP, et al. *Astrophys. J. Lett.* 826:L13 (2016)
61. Connaughton V, et al. *Astrophys. J. Lett.* 826:L6 (2016)
62. Veres P, et al. *Astrophys. J. Lett.* 827:L34 (2016)
63. Greiner J, Burgess JM, Savchenko V, Yu H-F. *Astrophys. J. Lett.* 827:L38 (2016)
64. Verrecchia F, et al. *Astrophys. J. Lett.* 847:L20 (2017)
65. Goldstein A, et al. *Astrophys. J. Lett.* 846:L5 (2017)
66. Bhalerao V, et al. *Astrophys. J. Lett.* 845:152 (2017)
67. Abbott BP, et al. *Astrophys. J. Lett.* 848:L13 (2017)
68. Goldstein A, et al. *Astrophys. J. Lett.* 848:L14 (2017)
69. Coulter DA, et al. *Science* 358:1556 (2017)
70. Troja E, et al. *Nature* 551:71 (2017)
71. Hallinan G, et al. *Science* 358:1579 (2017)
72. Abbott BP, et al. *Phys. Rev. X* 9:011001 (2019)
73. Gottlieb O, Nakar E, Piran T, Hotokezaka K. *Mon. Not. R. Astron. Soc.* 479:588 (2018)
74. Ioka K, Nakamura T. *Prog. Theor. Exp. Phys.* 2018:043E02 (2018)
75. Mooley KP, et al. *Nature* 554:207 (2018)
76. Lazzati D, et al. *Phys. Rev. Lett.* 120:241103 (2018)
77. Margutti R, et al. *Astrophys. J. Lett.* 856:L18 (2018)
78. Troja E, et al. *Mon. Not. R. Astron. Soc.* 478:L18 (2018)
79. Mooley KP, et al. *Nature* 561:355 (2018)
80. Beniamini P, Petropoulou M, Barniol Duran R, Giannios D. *Mon. Not. R. Astron. Soc.* 483:840 (2019)
81. Metzger BD. arXiv:1710.05931 [astro-ph] (2017)
82. Gupte N, Bartos I. arXiv:1808.06238 [astro-ph] (2018)
83. Bartos I, et al. *Mon. Not. R. Astron. Soc.* 485:4150 (2019)
84. Aglietta M, et al. *Nuovo Cim. C* 12:75 (1989)
85. Aso Y, et al. *Class. Quantum Gravity* 25:114039 (2008)
86. Pradier T. *Nucl. Instrum. Methods A* 602:268 (2009)
87. van Elewyck V, et al. *Int. J. Mod. Phys. D* 18:1655 (2009)
88. Pagliaroli G, Vissani F, Coccia E, Fulgione W. *Phys. Rev. Lett.* 103:031102 (2009)
89. Baret B, et al. *Astropart. Phys.* 35:1 (2011)
90. Baret B, et al. *Phys. Rev. D* 85:103004 (2012)
91. Bartos I, et al. arXiv:1810.11467 [astro-ph] (2018)
92. Bartos I, Finley C, Corsi A, Márka S. *Phys. Rev. Lett.* 107:251101 (2011)
93. Adrián-Martínez S, et al. *J. Cosmol. Astropart. Phys.* 6:008 (2013)
94. Aartsen MG, et al. *Phys. Rev. D* 90:102002 (2014)
95. Abbott BP, et al. *Phys. Rev. X* 6:041015 (2016)
96. Adrián-Martínez S, et al. *Phys. Rev. D* 93:122010 (2016)
97. Albert A, et al. *Phys. Rev. D* 96:022005 (2017)
98. Aab A, et al. *Phys. Rev. D* 94:122007 (2016)
99. Albert A, et al. *Astrophys. J.* 870:134 (2019)
100. Albert A, et al. *Astrophys. J. Lett.* 850:L35 (2017)
101. Albert A, et al. *Eur. Phys. J. C* 77:911 (2017)
102. Abbott BP, et al. *Living Rev. Relativ.* 21:3 (2018)
103. Kimura SS, Murase K, Mészáros P, Kiuchi K. *Astrophys. J. Lett.* 848:L4 (2017)
104. Ioka K, Nakamura T. *Mon. Not. R. Astron. Soc.* 487:4884 (2019)
105. Murase K, et al. *Astrophys. J.* 854:60 (2018)
106. Kimura SS, et al. *Phys. Rev. D* 98:043020 (2018)
107. Fang K, Metzger BD. *Astrophys. J.* 849:153 (2017)
108. Baikal-GVD Collab. arXiv:1810.10966 [astro-ph.HE] (2018)
109. Murase K, Inoue Y, Dermer CD. *Phys. Rev. D* 90:023007 (2014)

Annu. Rev. Nucl. Part. Sci. 2019.69:477-506. Downloaded from www.annualreviews.org
Access provided by University of Florida - Smathers Lib - Gainesville on 04/01/20. For personal use only.

110. Dermer CD, Murase K, Inoue Y. *J. High Energy Astrophys.* 3/4:29 (2014)
111. Reimer A, Boettcher M, Buson S. arXiv:1812.05654 [astro-ph] (2018)
112. Rodrigues X, et al. *Astrophys. J. Lett.* 874:L29 (2018)
113. Blandford RD, Znajek RL. *Mon. Not. R. Astron. Soc.* 179:433 (1977)
114. Farrar GR, Gruzinov A. *Astrophys. J.* 693:329 (2009)
115. Murase K. *AIP Conf. Proc.* 1065:201 (2008)
116. Wang X-Y, Liu R-Y, Dai Z-G, Cheng KS. *Phys. Rev. D* 84:081301 (2011)
117. Dai L, Fang K. *Mon. Not. R. Astron. Soc.* 469:1354 (2017)
118. Senno N, Murase K, Mészáros P. *Astrophys. J.* 838:3 (2017)
119. Lunardini C, Winter W. *Phys. Rev. D* 95:123001 (2017)
120. Burrows DN, et al. *Nature* 476:421 (2011)
121. Kobayashi S, Laguna P, Phinney ES, Mészáros P. *Astrophys. J.* 615:855 (2004)
122. Haas R, Shcherbakov RV, Bode T, Laguna P. *Astrophys. J.* 749:117 (2012)
123. Smith N. *Annu. Rev. Astron. Astrophys.* 52:487 (2014)
124. Murase K. *Phys. Rev. D* 97:081301 (2018)
125. Murase K, Thompson TA, Lacki BC, Beacom JF. *Phys. Rev. D* 84:043003 (2011)
126. Petropoulou M, et al. *Mon. Not. R. Astron. Soc.* 470:1881 (2017)
127. Margutti R, et al. *Astrophys. J.* 780:21 (2014)
128. Ackermann M, et al. *Astrophys. J.* 807:169 (2015)
129. Murase K, et al. *Astrophys. J.* 874:80 (2019)
130. Katz B, Sapir N, Waxman E. arXiv:1106.1898 [astro-ph] (2011)
131. Kashiyama K, et al. *Astrophys. J. Lett.* 769:L6 (2013)
132. Fryer CL, Woosley SE, Heger A. *Astrophys. J.* 550:372 (2001)
133. Dimmelmeier H, Ott CD, Marek A, Janka H-T. *Phys. Rev. D* 78:064056 (2008)
134. Ott CD, et al. *Phys. Rev. D* 86:024026 (2012)
135. Radice D, et al. *Astrophys. J. Lett.* 876:L9 (2019)
136. Piro AL, Thrane E. *Astrophys. J.* 761:63 (2012)
137. Cutler C. *Phys. Rev. D* 66:084025 (2002)
138. Stella L, Dall'Osso S, Israel G, Vecchio A. *Astrophys. J. Lett.* 634:L165 (2005)
139. Kashiyama K, et al. *Astrophys. J.* 818:94 (2016)
140. Mészáros P. *Rep. Prog. Phys.* 69:2259 (2006)
141. Kumar P, Zhang B. *Phys. Rep.* 561:1 (2014)
142. Waxman E, Bahcall JN. *Phys. Rev. Lett.* 78:2292 (1997)
143. Murase K, Nagataki S. *Phys. Rev. D* 73:063002 (2006)
144. Baerwald P, Hummer S, Winter W. *Phys. Rev. D* 83:067303 (2011)
145. Bustamante M, Murase K, Winter W, Heinze J. *Astrophys. J.* 837:33 (2017)
146. Bustamante M, Baerwald P, Murase K, Winter W. *Nat. Commun.* 6:6783 (2015)
147. Baerwald P, Bustamante M, Winter W. *Astrophys. J.* 768:186 (2013)
148. Globus N, Allard D, Mochkovitch R, Parizot E. *Mon. Not. R. Astron. Soc.* 451:751 (2015)
149. Biehl D, Boncioli D, Fedynitch A, Winter W. *Astron. Astrophys.* 611:A101 (2018)
150. Gupta N, Zhang B. *Astropart. Phys.* 27:386 (2007)
151. Senno N, Murase K, Mészáros P. *Phys. Rev. D* 93:083003 (2016)
152. Tamborra I, Ando S. *Phys. Rev. D* 93:053010 (2016)
153. Murase K, Ioka K, Nagataki S, Nakamura T. *Phys. Rev. D* 78:023005 (2008)
154. Zhang BT, et al. *Phys. Rev. D* 97:083010 (2018)
155. Boncioli D, Biehl D, Winter W. *Astrophys. J. Lett.* 872:110 (2018)
156. Zhang BT, Murase K. arXiv:1812.10289 [astro-ph] (2018)
157. Aartsen MG, et al. *Astrophys. J.* 824:115 (2016)
158. Murase K. *Phys. Rev. D* 78:101302 (2008)
159. Wang X-Y, Dai Z-G. *Astrophys. J. Lett.* 691:L67 (2009)
160. Zhang B, Kumar P. *Phys. Rev. Lett.* 110:121101 (2013)
161. Murase K, Ioka K. *Phys. Rev. Lett.* 111:121102 (2013)

Annu. Rev. Nucl. Part. Sci. 2019.69:477-506. Downloaded from www.annualreviews.org
Access provided by University of Florida - Smathers Lib - Gainesville on 04/01/20. For personal use only.

162. Bahcall JN, Mészáros P. *Phys. Rev. Lett.* 85:1362 (2000)
163. Beloborodov AM. *Mon. Not. R. Astron. Soc.* 407:1033 (2010)
164. Murase K, Kashiyama K, Mészáros P. *Phys. Rev. Lett.* 111:131102 (2013)
165. Bartos I, Beloborodov AM, Hurley K, Márka S. *Phys. Rev. Lett.* 110:241101 (2013)
166. Kobayashi S, Mészáros P. *Astrophys. J.* 589:861 (2003)
167. Piro AL, Pfahl E. *Astrophys. J.* 658:1173 (2007)
168. Kiuchi K, Shibata M, Montero PJ, Font JA. *Phys. Rev. Lett.* 106:251102 (2011)
169. Fryer CL, Holz DE, Hughes SA. *Astrophys. J.* 565:430 (2002)
170. Ott CD, et al. *Phys. Rev. Lett.* 106:161103 (2011)
171. Suwa Y, Murase K. *Phys. Rev. D* 80:123008 (2009)
172. Sago N, et al. *Phys. Rev. D* 70:104012 (2004)
173. Corsi A, Mészáros P. *Astrophys. J.* 702:1171 (2009)
174. Mészáros P, Waxman E. *Phys. Rev. Lett.* 87:171102 (2001)
175. Razzaque S, Mészáros P, Waxman E. *Phys. Rev. Lett.* 93:181101 (2004). Erratum. *Phys. Rev. Lett.* 94:109903 (2005)
176. Ando S, Beacom JF. *Phys. Rev. Lett.* 95:061103 (2005)
177. Iocco F, Murase K, Nagataki S, Serpico PD. *Astrophys. J.* 675:937 (2008)
178. Campana S, et al. *Nature* 442:1008 (2006)
179. Denton PB, Tamborra I. *Astrophys. J.* 855:37 (2018)
180. Thompson TA, Chang P, Quataert E. *Astrophys. J.* 611:380 (2004)
181. Kashiyama K, et al. *Astrophys. J.* 818:94 (2016)
182. Margalit B, et al. *Mon. Not. R. Astron. Soc.* 481:2407 (2018)
183. Metzger BD, Vurm I, Hascoet R, Beloborodov AM. *Mon. Not. R. Astron. Soc.* 437:703 (2014)
184. Murase K, Kashiyama K, Kiuchi K, Bartos I. *Astrophys. J.* 805:82 (2015)
185. Margutti R, et al. *Astrophys. J.* 864:45 (2018)
186. Renault-Tinacci N, Kotera K, Neronov A, Ando S. *Astron. Astrophys.* 611:A45 (2018)
187. Blasi P, Epstein RI, Olinto AV. *Astrophys. J. Lett.* 533:L123 (2000)
188. Arons J. *Astrophys. J.* 589:871 (2003)
189. Murase K, Mészáros P, Zhang B. *Phys. Rev. D* 79:103001 (2009)
190. Fang K, Kotera K, Murase K, Olinto AV. *Phys. Rev. D* 90:103005 (2014)
191. Fang K, et al. *Astrophys. J.* 878:34 (2019)
192. Paczynski B. *Astrophys. J. Lett.* 308:L43 (1986)
193. Eichler D, Livio M, Piran T, Schramm DN. *Nature* 340:126 (1989)
194. Berger E. *Annu. Rev. Astron. Astrophys.* 52:43 (2014)
195. Janka H-T, Eberl T, Ruffert M, Fryer CL. *Astrophys. J. Lett.* 527:L39 (1999)
196. Rosswog S. *Astrophys. J.* 634:1202 (2005)
197. Foucart F. *Phys. Rev. D* 86:124007 (2012)
198. Kyutoku K, et al. *Phys. Rev. D* 88:041503 (2013)
199. Kyutoku K, et al. *Phys. Rev. D* 92:044028 (2015)
200. Kiuchi K, et al. *Phys. Rev. D* 92:064034 (2015)
201. Paschalidis V, Ruiz M, Shapiro SL. *Astrophys. J. Lett.* 806:L14 (2015)
202. Ruiz M, Shapiro SL, Tsokaros A. *Phys. Rev. D* 98:123017 (2018)
203. Shibata M, et al. *Phys. Rev. D* 96:123012 (2017)
204. Margalit B, Metzger BD. *Astrophys. J. Lett.* 850:L19 (2017)
205. Coughlin MW, Dietrich T, Margalit B, Metzger BD. arXiv:1812.04803 [astro-ph] (2018)
206. Abbott BP, et al. *Phys. Rev. Lett.* 121:161101 (2018)
207. Abbott BP, et al. *Nature* 551:85 (2017)
208. Margutti R, et al. *Astrophys. J. Lett.* 848:L20 (2017)
209. Biehl D, et al. *Mon. Not. R. Astron. Soc.* 476:1191 (2018)
210. Kocevski D, Omodei N, Vianello G. arXiv:1710.05450 [astro-ph] (2017)
211. Abdalla H, et al. *Astrophys. J. Lett.* 850:L22 (2017)
212. Belczynski K, Kalogera V, Bulik T. *Astrophys. J.* 572:407 (2002)

Annu. Rev. Nucl. Part. Sci. 2019.69:477-506. Downloaded from www.annualreviews.org
Access provided by University of Florida - Smathers Lib - Gainesville on 04/01/20. For personal use only.

213. O'Leary RM, Kocsis B, Loeb A. *Mon. Not. R. Astron. Soc.* 395:2127 (2009)
214. Rodriguez CL, et al. *Phys. Rev. Lett.* 115:051101 (2015)
215. Hailey CJ, et al. *Nature* 556:70 (2018)
216. Fragione G, Kocsis B. *Phys. Rev. Lett.* 121:161103 (2018)
217. Ivanova N, et al. *Mon. Not. R. Astron. Soc.* 372:1043 (2006)
218. Bartos I, Kocsis B, Haiman Z, Márka S. *Astrophys. J.* 835:165 (2017)
219. Stone NC, Metzger BD, Haiman Z. *Mon. Not. R. Astron. Soc.* 464:946 (2017)
220. Bartos I, et al. *Nat. Commun.* 8:831 (2017)
221. Yang Y, et al. *Astrophys. J.* 876:122 (2019)
222. Perna R, Lazzati D, Giacomazzo B. *Astrophys. J. Lett.* 821:L18 (2016)
223. Murase K, et al. *Astrophys. J. Lett.* 822:L9 (2016)
224. Kotera K, Silk J. *Astrophys. J. Lett.* 823:L29 (2016)
225. Moharana R, Razzaque S, Gupta N, Mészáros P. *Phys. Rev. D* 93:123011 (2016)
226. Kimura SS, Takahashi SZ, Toma K. *Mon. Not. R. Astron. Soc.* 465:4406 (2017)
227. Loeb A. *Astrophys. J. Lett.* 819:L21 (2016)
228. Dai L, McKinney JC, Miller MC. *Mon. Not. R. Astron. Soc.* 470:L92 (2017)
229. Beloborodov AM. *Mon. Not. R. Astron. Soc.* 438:169 (2014)
230. Ji S, et al. *Astrophys. J.* 773:136 (2013)
231. Xiao D, Mészáros P, Murase K, Dai Z-G. *Astrophys. J.* 832:20 (2016)
232. Amaro-Seoane P, et al. *Class. Quantum Gravity* 29:124016 (2012)
233. Evans CR, Iben I, Smarr L. *Astrophys. J.* 323:129 (1987)
234. Korol V, et al. *Mon. Not. R. Astron. Soc.* 470:1894 (2017)
235. Moiseev A (AMEGO Team). *Proc. Sci.* 301:798 (2018)
236. Sathyaprakash B, et al. *Class. Quantum Gravity* 29:124013 (2012). Erratum. *Class. Quantum Gravity* 30:079501 (2013)
237. Abbott BP, et al. *Class. Quantum Gravity* 34:044001 (2017)
238. Alves Batista R, et al. arXiv:1903.06714 [astro-ph] (2019)
239. Aartsen MG, et al. arXiv:1412.5106 [astro-ph] (2014)
240. Abe K, et al. (Hyper-Kamiokande Proto-Collab.) arXiv:1805.04163 [physics.ins-det] (2018)
241. Albert A, et al. arXiv:1902.08429 [astro-ph] (2019)
242. CTA Consort. *Science with the Cherenkov Telescope Array*. Singapore: World Sci. (2019)

Annu. Rev. Nucl. Part. Sci. 2019.69:477-506. Downloaded from www.annualreviews.org
Access provided by University of Florida - Smathers Lib - Gainesville on 04/01/20. For personal use only.

Annual Review of Nuclear and Particle Science

Volume 69, 2019

Contents

Annu. Rev. Nucl. Part. Sci. 2019.69:477-506. Downloaded from www.annualreviews.org
Access provided by University of Florida - Smathers Lib - Gainesville on 04/01/20. For personal use only.

Errata

An online log of corrections to *Annual Review of Nuclear and Particle Science* articles may be found at http://www.annualreviews.org/errata/nucl

Annu. Rev. Nucl. Part. Sci. 2019.69:477-506. Downloaded from www.annualreviews.org
Access provided by University of Florida - Smathers Lib - Gainesville on 04/01/20. For personal use only.